

IMPERIAL COLLEGE LONDON

Watching the Interstellar Clocks

Pulsar Observations with Future and Proposed
Cherenkov Telescope Arrays

Ian Proudlock

2009/2010

Imperial College
London



"The more you read and learn, the less your adversary will know." -Sun Tzu, The Art of War

Abstract

We have simulated the performance of two Imaging Atmospheric Cherenkov Telescope Arrays, CTA and 5@5, and examined their observational potential for pulsar observations, their ability to detect giant pulses in the Crab Pulsar and the signatures of different emission modes of the Crab. Our results indicate that both CTA and 5@5 will be significantly better than current instruments for pulsar observations in the gamma range, with detection rates many orders of magnitude higher than those currently achieved and that, if it performs as predicted, 5@5 would be the superior pulsar observatory of the two arrays. We have found that the direct observation of giant pulses in a blind search will be impractical due to background coincidences. Assuming that giant pulses are coincidental in the gamma and radio regimes, timing data from the radio range could be used to localise gamma ray giant pulses. This would allow for a better chance of observing and correctly identifying giant pulses. Detection of giant pulses through Statistical Interval Analysis will be possible, if the array can detect pulsed photons from the Crab at a rate of 0.1 Hz or greater. We have identified a possible giant pulse only emission mode for the gamma range with an increased giant pulse frequency and average magnitude that reproduces the available data, and identified signatures for this emission mode for both standard observations, and under Statistical Interval Analysis.

Wir haben die Eigenschaften von zwei Cherenkov Licht Teleskope Arrays, CTA und 5@5, sowie die Möglichkeiten für die Beobachtung von Pulsaren, großen Pulsen und verschiedenen Emissions-Modi des Krebs Pulsars untersucht. Unsere Ergebnisse zeigen, dass beide, CTA und 5@5, viel besser als derzeitige Instrumente für das Beobachten von Pulsaren im Gammabereich geeignet sind, denn ihre Detektionsraten liegen viele Größenordnungen höhere über denen, die zur Zeit möglich sind. Wenn sie wie vorhergesagt funktioniert, wird das 5@5 Array die bessere Instrument für die Beobachtung von Pulsaren. Wir haben herausgefunden, dass die direkte Beobachtung von großen Pulsen in Rohdaten unmöglich ist, weil das Signal von Koinzidenzen überlagert ist. Wenn große Pulse im Radio- und Gammabereich auftreten, kann man die Radiodaten benutzen, um im Gammabereich große Pulse zu lokalisieren. In diesem Fall sind die Möglichkeiten, dass man große Pulse detektieren und identifizieren kann, erhöht. Die Detektion von großen Pulsen ist durch eine statistische Intervall Analyse möglich, wenn das Array gepulste Photonen mit einer Frequenz von 0.1 Hz oder mehr detektieren kann. Wir haben einen möglichen Emissions-Modus entdeckt, der nur große Pulse mit höherer Frequenz und Größenordnung benutzt und die verfügbaren Daten reproduziert. Wir haben Signaturen für diesen Emissions-Modus in beiden Beobachtungen und mit der statistischen Intervall Analyse gefunden.

Table of Contents

| | |
|---|----|
| Abstract..... | 3 |
| List of Figures | 6 |
| List of Tables | 6 |
| List of Equations..... | 6 |
| Preface | 7 |
| List of Abbreviations | 8 |
| 1.0 Introduction | 9 |
| 1.1 Current Methods for Detecting Gamma Photons..... | 9 |
| 1.2 Pulsars..... | 11 |
| 1.3 The Cherenkov Telescope Array (CTA)..... | 12 |
| 1.4 The 5 GeV Threshold Array at 5 km above sea level array (5@5) | 13 |
| 1.5 The Crab Pulsar | 14 |
| 1.6 The Vela Pulsar..... | 16 |
| 1.7 Giant Pulses..... | 16 |
| 2.0 Preliminary Work: Detection and Background Rates | 17 |
| 2.1 Method for Calculating the Detection Rate..... | 17 |
| 2.2 Method for Calculating the Background Rate | 22 |
| 2.3 Results: Detection Rates | 23 |
| 2.4 Results: Background Rates..... | 25 |
| 2.5 Discussion..... | 26 |
| 3.0 Method: Modelling the Crab Pulsar..... | 27 |
| 3.1 Structure of the Model | 27 |
| 3.2 Simplifications and Assumptions | 29 |
| 3.3 Giant Pulse Simulator..... | 30 |
| 3.4 Direct Observations | 31 |
| 3.5 Variations to the Model: Statistical Interval Analysis | 33 |
| 3.6 Variations to the Model: Other Emission Modes | 34 |
| 3.7 Testing of the Model..... | 35 |
| 4.0 Results..... | 36 |
| 4.1 Simulated Light Curves..... | 36 |
| 4.2 Direct Observations of Giant Pulses..... | 43 |
| 4.3 Statistical Interval Analysis..... | 46 |
| 4.4 Signatures of Emission Modes | 50 |

| | | |
|-----|--|----|
| 5.0 | Discussion..... | 55 |
| 5.1 | Simulated Light Curves..... | 55 |
| 5.2 | Direct Observation of Giant Pulses | 56 |
| 5.3 | Statistical Interval Analysis..... | 57 |
| 5.4 | Emission Mode Signatures..... | 58 |
| 6.0 | Conclusions | 59 |
| 6.1 | General Observations | 59 |
| 6.2 | Comparison of the Arrays | 60 |
| 7.0 | Extensions and Refinements..... | 61 |
| 7.1 | Refinements to the Current Model..... | 61 |
| 7.2 | Model of the Vela Pulsar..... | 63 |
| 7.3 | Application to other Phenomena..... | 64 |
| | Acknowledgments..... | 65 |
| | Bibliography | 66 |

List of Figures

| | |
|---|----|
| Figure 1: Development of a Cherenkov Light Cone | 10 |
| Figure 2: A diagram of a possible CTA South arrangement | 13 |
| Figure 3: Effective Area curve for 5@5 | 14 |
| Figure 4: Pulse Profiles of the Crab Pulsar in Different Energy Bands | 15 |
| Figure 5: Spectra for the Vela Pulsar from the Fermi LAT | 18 |
| Figure 6: Fermi and MAGIC spectra for the Crab Pulsar | 19 |
| Figure 7: Plot of Fermi and Magic data points compared to the Fermi spectrum | 19 |
| Figure 8: Hybrid spectra for the Crab Pulsar | 20 |
| Figure 9: Fitting of the CTA LET curve to the CTA sub-array data points | 21 |
| Figure 10: The Effective Area Estimates for CTA and 5@5 | 22 |
| Figure 11: The Pulse Profile of the Crab Pulsar above 100 MeV | 28 |
| Figure 12: Flow Chart of the Main Program | 29 |
| Figure 13: Flow chart of the structure of the SIA model | 34 |
| Figure 14: The results of the tests of the giant pulse magnitude generator | 36 |
| Figure 16: CTA Raue pulse profiles | 37 |
| Figure 17: Pulse profile development for the Fermi spectrum with CTA Raue | 40 |
| Figure 18: 5@5 pulse profiles | 41 |
| Figure 19: SIA results for CTA Raue | 47 |
| Figure 20: SIA results for 5@5 | 49 |
| Figure 21: The pulse profile reconstructed only from background and giant pulse photons | 52 |
| Figure 22: CTA LET and CTA Raue pulse profiles for the giant pulse only emission mode | 53 |
| Figure 23: 5@5 pulse profiles for the giant pulse only emission mode | 54 |
| Figure 24: SIA results of CTA Raue observations of the Fermi spectrum with the giant pulse only emission mode | 54 |
| Figure 25: A giant pulse of the Crab recorded at multiple frequencies | 62 |
| Figure 26: Fermi pulse profile for the Vela pulsar | 63 |

List of Tables

| | |
|--|----|
| Table 1: Photon Detection Rates for 5@5 and CTA | 24 |
| Table 2: Detection Rates for Fermi's LAT and MAGIC | 25 |
| Table 3: Background Rates for each Instrument in the range 1 to 100 GeV | 26 |
| Table 4: Defined regions of the pulse and proportions of giant pulses that occur in them | 32 |
| Table 5: Expected number of direct observations for CTA LET | 44 |
| Table 6: Expected number of direct observations for CTA Abramowski | 44 |
| Table 7: Expected number of direct observations for CTA Raue | 45 |
| Table 8: Expected number of direct observations for 5@5 | 45 |

List of Equations

| | |
|--|----|
| Equation 1: The Cherenkov Condition | 11 |
| Equation 2: Photon Detection Count | 31 |
| Equation 3: Magnitude Probability Calculator | 32 |

Preface

This work was performed at the University of Hamburg Astro-particle Physics Group in the Deutsches Elektronen Synchrotron (DESY) facility in Hamburg from November 2009 to June 2010. The project was supervised by Professor D. Horns, who gave advice and guidance throughout the project, specifically suggesting the concept of Statistical Interval Analysis. My part in this project was performing the calculations for the detection and background rates, all calculations associated with the observational results presented here and writing the models of the Crab pulsar for building light curves and performing Statistical Interval Analysis, performing the simulations and the subsequent analysis and conclusions.

List of Abbreviations

5@5: 5GeV Threshold Array at 5km above sea level
ALMA: Atacama Large Millimeter/Sub-millimeter Array
CTA: Cherenkov Telescope Array
GeV: Giga-electron volt
GLAST: Gamma-ray Large Area Space Telescope
H.E.S.S.: High Energy Stereoscopic System
HEGRA: High Energy Gamma Ray Astronomy
IACT: Imagine Atmospheric Cherenkov Telescope
LAT: Large Area Telescope
LET: Low energy threshold
MAGIC: Major Atmospheric Gamma-ray Imaging Cherenkov telescope
MeV: Mega-electron volt
SIA: Statistical Interval Analysis
TeV: Tera-electron volt

1.0 Introduction

In 1968 the Whipple Cherenkov Telescope was built at the Mount Hopkins, now Fred Lawrence Whipple, Observatory (1), heralding the birth of ground based gamma ray astronomy. This telescope went on to discover the first extra-galactic TeV gamma rays (2), as well as the first TeV gamma photons from the Crab Nebula (2). One year before the construction of the Whipple 10m telescope, the first detection of a pulsar was made by J. Bell and A. Hewish (3). Since then, numerous pulsars have been detected, including several that emit in the gamma energy range, such as the Crab and Vela Pulsars (4). Current technologies, however, limit the observation of pulsars in the gamma range, hindering the development of models of these enigmatic phenomena.

The best instruments to date for observing gamma ray pulsars are the Large Area Telescope on the Fermi Space Telescope, formerly known as the GLAST mission, and the MAGIC Cherenkov Telescopes on La Palma. MAGIC recently confirmed the detection of pulsed emission from the Crab Pulsar at energies above 25 GeV (5). Fermi has opened up the field of gamma pulsar astronomy, with less than 10 gamma pulsars known before its launch (6), as compared to the 46 published in the First Fermi Large Area Telescope Catalog of Gamma-Ray Pulsars (4).

The aims of this project are to assess the observational potential of two telescope arrays¹, one currently being designed and one proposed, with regards to gamma ray pulsars, with specific attention to whether the telescopes will be able to detect giant pulses in the Crab Pulsar and the arrays' ability to reconstruct the pulse profile of the Crab pulsar.

The following sub-sections will give a general overview of the current methods and technologies for observing the gamma ray sky, and an introduction to pulsars. The specific instruments and targets that this project will examine will be discussed in greater detail in dedicated sub-sections.

1.1 Current Methods for Detecting Gamma Photons

The technologies available for detecting gamma ray photons can be divided into two classes; direct and indirect. One major obstacle to directly detecting gamma rays is that they are absorbed in the atmosphere. Consequently, direct detection experiments are usually space, rocket or balloon borne. This presents a fundamental limitation, as the size of the experiments is limited to the lift capacity of the balloon or spacecraft. The Fermi space telescope's Large Area Telescope, for example, has an effective area of around 0.8m^2 . (7) Especially for higher energy events this reduces the rate of data collection massively, limiting their effective observational range of these instruments to the lower gamma range, up to a few tens of GeV.

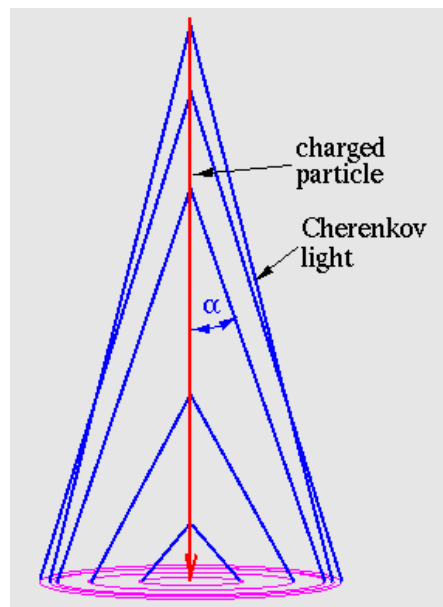
¹ For clarification, the terms array and telescope are often both used to identify an array of telescopes in papers, i.e. the H.E.S.S. telescope actually consists of four individual telescopes in an array. In this project, the word telescope means an individual mirror/ camera arrangement, and an array or instrument refers to a collection of telescopes.

Indirect methods of gamma ray detection rely on detecting secondary particles produced when the gamma photons enter the atmosphere. Gamma rays entering the atmosphere are absorbed through the formation of electron/positron showers (8). These particle showers can be detected at ground level using Air-Shower Arrays. These arrays have to be very large to cover all the area of the shower at sea level, which can be of the order 0.5km^2 (8). To allow the detection of the particles at ground level they must be created with sufficient energy, requiring a primary gamma-ray with an energy of around 10 TeV (8). This limit is far too high to allow for pulsar observation, effectively eliminating this technique as a useful tool for this project.

A further method, by far the most promising for pulsar observation, of indirectly detecting gamma rays is the detection of Cherenkov light created by the secondary particle cascade. Gamma ray photons entering the atmosphere with sufficient energy can create electron/positron pairs that are travelling at a speed greater than the speed of light in air. If the particles fulfil the Cherenkov condition, shown in Equation 1, requiring the electrons and positrons in the air shower to have an energy of roughly 21 MeV or greater (8), they will emit Cherenkov radiation in a manner depicted by Figure 1, producing a flash of blue with a duration of a few nanoseconds at ground level. Despite the massive night-sky background of around $10^{12}\text{ ph m}^{-2}\text{ s}^{-1}\text{ sr}^{-1}$ (8), the short duration of the Cherenkov pulse, along with its small dispersion allows for the detection of the Cherenkov photon signal above the background.

Figure 1: Development of a Cherenkov Light Cone

Diagram showing the development of a Cherenkov light cone around a charged particle moving through the atmosphere at or above the local speed of light. The Cherenkov angle α is dependent on the density of the atmosphere, so varies with height. The illuminated circle under the shower is shown in pink circles.



The mirrors of the Imaging Atmospheric Cherenkov Telescope (IACT) reflect the detected photons to a central camera, which uses photo multiplier tubes to record an image of the shower. To trigger an individual telescope, a set number, which varies with the individual array, of photo-multiplier tubes must detect a set number of photons within a set time frame. In the case of an array, a set number of telescopes must trigger in order for an event to be recorded as a gamma-photon event.

Stereoscopic imaging like this, with 2 or more telescopes acting in concert, allows for very good angular resolution, background rejection and a reasonable energy resolution. Stereoscopic IACT arrays were pioneered with the HEGRA Array (9).

Equation 1: The Cherenkov Condition

$$\cos(\theta_c) = \frac{1}{n\beta}$$

Where θ_c is the angle of the Cherenkov light cone from the incident ray, n is the refractive index of the medium, and β is the velocity of the particle divided by the speed of light in the medium.

The use of multiple images improves the ability to detect the source of the gamma rays. The primary axes of the shower images, the longer axis of the elliptical image, point back to the source. With multiple axes, the source can be pinpointed to the intersection point, within measurement errors, rather than just along a line. The stereoscopic system improves the reconstruction of all the shower parameters (10), meaning that the errors in the characterisation of the gamma photon are reduced.

The defining characteristic of a telescope or array, which determines its sensitivity etc, is its effective area. This is the area over which a signal can arrive and trigger the telescope or array, and is a function of the energy of the primary photon. For Cherenkov telescopes, the effective area curve (as a function of energy) can be characterised as a steep rise until a specific energy, followed by a relatively flat section. Initially the area rises rapidly, as the Cherenkov light pool becomes strong enough to trigger the array over a larger portion of its area. At first, a photon's light pool must arrive approximately centrally to the array in order to cause enough triggering events (i.e. triggering the correct number of photo-multiplier tubes in the correct number of telescopes) as the photon density is low. As the density increases, the possibility of triggering with only a partial area of the light pool, or with the less densely packed outer regions of an array increases the effective area. After reaching the threshold energy where all of the telescopes can trigger, the effective area is effectively constrained to the area of the array or telescope itself plus a band with the width of a Cherenkov radius (the radius of the light pool illuminated by a photon) around the array. As the Cherenkov radius increases with the primary gamma energy, this causes a slight growth in the effective area as the energy increases further.

1.2 Pulsars

Pulsars are highly magnetised rotating neutron stars, formed by a core collapse super-nova. Neutron stars are extremely dense, with densities as high as 10^{14} g cm⁻³, comparable to the densities in atomic nuclei (11), and have very powerful magnetic fields of around 10^{12} Gauss. (11) They produce electromagnetic radiation through their spin-down power, as the pulsar's rotation slows, which is strong in the GeV band. (12) The rotation sweeps emitted beams of electromagnetic radiation through space which, if they intersect with the Earth, manifest as pulses of radio, optical, X-ray and/or gamma radiation.

The emission spectra of pulsars are formed of a power law distribution with an exponential or super exponential cut off. The cut off is produced by the interaction of high energy photons with the

magnetic field of the pulsar itself. If they are of sufficient energy, the photons undergo pair production. This cut off energy is dependent on the magnetic field of the pulsar, and curtails the energy range that is observable. The exact mechanism of the emission from pulsars is still disputed, with several different models, such as the polar cap and slot gap models, existing. Gamma ray emissions may be able to help differentiate between the different models, allowing for a more complete understanding of both pulsars and extreme forms of matter.

It is currently assumed that pulsars emit gamma photons in the same manner as their radio photons, a pulsed component, with any additional features, such as giant pulses, above this. The pulse profiles recorded for pulsars that emit in both regions often show substantial similarities, with a gamma peak for each radio peak, although often with a broadening of the pulse. Almost all pulsars with both radio and gamma components follow this trend, with the gamma peak lagging the radio peak slightly. (6) With the current rate of photon detection however, it is possible that the emission of gamma ray photons follows an entirely different pattern. In the case of the Crab², for example, it is possible that gamma ray photons are only emitted during giant pulses. This project will aim to determine whether the next generation telescopes will be able to differentiate between different emission modes, and what the signatures of these modes might be.

1.3 The Cherenkov Telescope Array (CTA)

Current IACT arrays are fairly small affairs, with few telescopes (4 in the case of H.E.S.S. and 2 in the case of MAGIC), which consequently limits their effective areas, and thus the rate of photon detections. The Cherenkov Telescope Array (CTA) will overcome this limitation by simply increasing the number of telescopes in the array. The CTA is currently being designed by an international collaboration, and will consist of two arrays, CTA North and CTA South (13). CTA North in the Northern Hemisphere will be a low energy threshold array (13), primarily intended for the study of extragalactic sources. Although the Crab is in the northern hemisphere, due to the CTA North array's ill suitability to pulsar observations, we will instead focus on CTA South, which will consist of 50-100 telescopes in an array spread over an area between 1 and 10 square kilometres, depending on which of the possible configurations is chosen as the final design. The array will probably contain a mixture of different sized telescopes, from small 10m instruments to giant 32m diameter telescopes. Multiple different possible array configurations are currently being simulated to optimise the performance of the array. The CTA project is aimed at improving our knowledge of the gamma ray sky, both by identifying more gamma-ray sources, and by increasing our knowledge of the currently known sources.

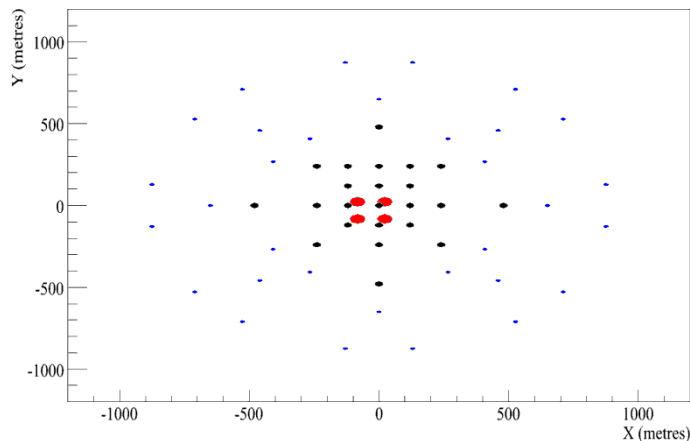
The configurations currently being simulated, termed sub-arrays, can be divided into two broad categories based on the anticipated energy thresholds. The first group are the larger sub-arrays, without the larger type telescopes. Without the large telescopes, the energy threshold of the array is raised to around 100 GeV, based on the current simulation data. These sub-arrays, which are termed High Energy Threshold (HET) sub-arrays in this report, are highly unsuited for pulsar observations, as

² Unless otherwise stated, any reference to “(the) Crab” refers to the pulsar itself, not the nebula/pulsar system. Additionally references to “(the) Vela” refer to the Vela pulsar.

they cannot effectively observe the energy range that pulsars emit in, and have been disregarded for the purposes of this project.

Figure 2: A diagram of a possible CTA South arrangement

This diagram shows the layout of Sub-Array E, a Low Energy Threshold array. The different coloured circles represent telescopes of different sizes (Red are 23m diameter, black 12m and blue 7m). The central core is clearly visible. Image from “MC Production Run Analysis: Durham Status” talk by Sam Nolan and Cameron Rulten, Leeds June 2006.



The second category of sub-arrays, which are termed Low Energy Threshold (LET) sub-arrays in this project, have a dense central core of telescopes, including the large 23 or 32 metre diameter telescopes. This core lowers the energy threshold of the array to something of the order of tens of GeV. This places the higher energy end of pulsar emissions within reach of the CTA. Coupled with the large effective area that the array will offer, CTA will give a radical increase in fluence sensitivity to gamma ray sources, allowing for the detection of new sources and vastly improving the rate of data collection on currently known objects.

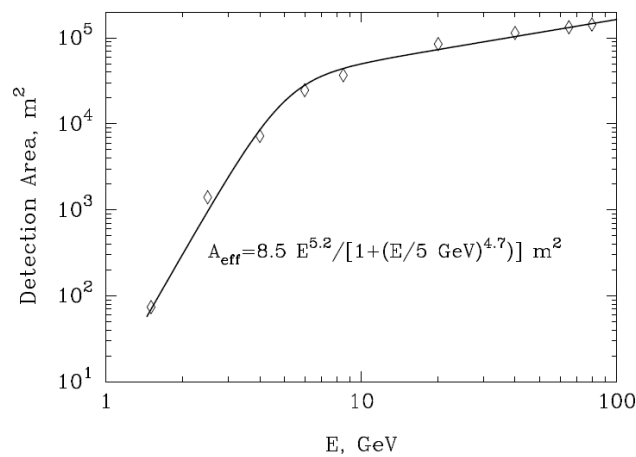
1.4 The 5 GeV Threshold Array at 5 km above sea level array (5@5)

The 5 GeV Threshold Array at 5km above sea level (5@5) array was proposed in 2001 by Aharonian et al, and aims to take advantage of the increase in Cherenkov photon density in the air shower higher in the atmosphere. This allows for the energy threshold to be drastically reduced, as the density of photons required for the telescope to trigger, which is independent of the altitude of the observation, corresponds to a lower energy. This could potentially reduce the energy threshold to as low as 5 GeV, which is a massive improvement on current ground based telescope energy thresholds. (14) The core concept behind the telescope is to bridge the energy gap between the energy ranges of space based gamma ray telescopes, which typically cover from the MeV range through to a few tens of GeV, and ground based Cherenkov telescopes, which usually cover from a hundreds of GeV up to the TeV range. (14)

The array would consist of between 4 and 6 telescopes, arranged in formation to achieve an optimal balance of performance characteristics. The simulations used to provide the data in the paper were based on the model of a 4 telescopes arranged in a square with sides of length 100 metres with a fifth central telescope. (14) The simulations produced the effective area curve shown below in Figure 3. The proposed site for the experiment is the Atacama Desert in Chile, taking advantage of the infrastructure already in place for the ALMA experiment. (14)

Figure 3: Effective Area curve for 5@5

Plot of the effective area of the proposed 5@5 telescope array as a function of energy, as simulated by Aharonian et al in the 5@5 - a 5 GeV energy threshold array of imaging atmospheric Cherenkov telescopes at 5 km altitude paper. The rapid rise and subsequent slowly increasing form discussed in Section 1.1 can clearly be seen. The turning point is at around 5 GeV, contributing to the name of the array.



The lower energy threshold of the array reduces the impact of the energy cut-off in the pulsars spectrum, making 5@5 ideally suited for pulsar observations. It should be stressed however, that the simulations of 5@5 are not as developed as those of the CTA, so the data available may be an optimistic view, and an actual array built to fulfil this concept may not perform as well. As such, the 5@5 case should be looked on as a best case scenario. It should also be noted that there doesn't appear to be any interest in taking the 5@5 concept through to construction, its inclusion in this project is primarily to provide a comparison and to examine what may be possible with IACT arrays as an observational tool for phenomena in the GeV range.

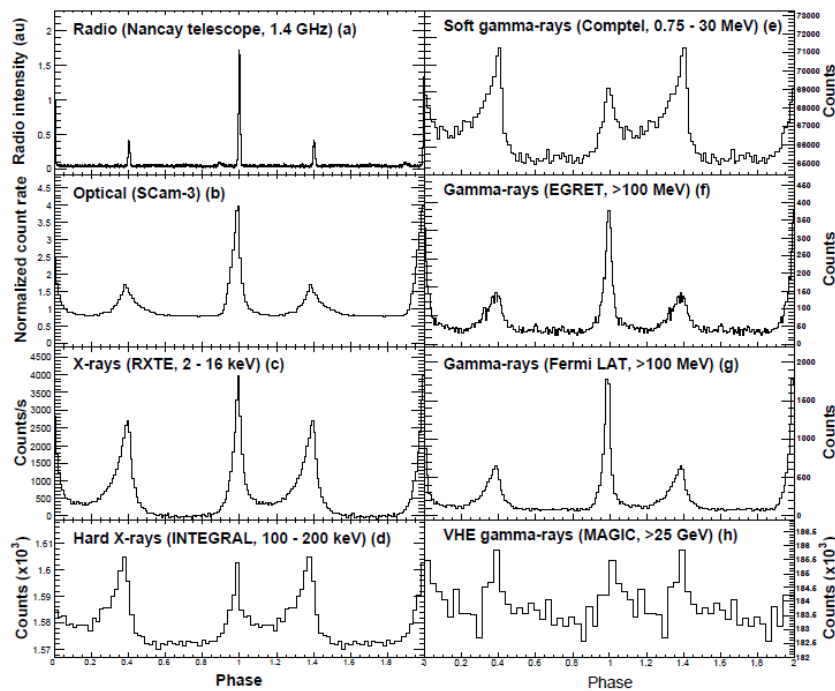
1.5 The Crab Pulsar

The Crab Pulsar is the remnant of a supernova that occurred in 1054, located approximately 2 kilo parsecs from Earth, (4) and forms the core of the Crab Nebula, as well as powering emission from the Nebula. The pulsar has a period of 33.08 milliseconds (15), with a dual peak, in the pulse, P1, the larger main pulse, and P2, a smaller inter pulse. The pulsar has been studied by both the MAGIC and Fermi LAT telescopes in the gamma range, (16) giving a high and very high energy view of the pulsar, which reveals some interesting characteristics. As shown in Figure 4, the morphology of the pulse

profile changes with increasing energy, with P2, the smaller pulse in the radio range, increasing in significance and size in relation to P1, the main radio pulse.

Figure 4: Pulse Profiles of the Crab Pulsar in Different Energy Bands

Plots of the pulse profile of the Crab from different telescopes at different energy ranges. The shift in the morphology of the pulses at higher energies can clearly be seen in the MAGIC pulse profile (h). The broadening of the pulses from the radio to the gamma bands can also be seen. Image from FERMI LARGE AREA TELESCOPE OBSERVATIONS OF THE CRAB PULSAR AND NEBULA The Astrophysical Journal, Volume 708, Issue 2, pp. 1254-1267 (2010).



The Crab Pulsar also emits giant pulses in the radio range. These events are very brief, sometimes as short as a few nanoseconds, (17) but can have a peak intensity of several thousand times that of an average pulse. The mechanism that produces these phenomena is still unknown, as is their relation to the standard pulses. Due to the similarity between the radio and gamma pulse profiles of the Crab pulsar, giant pulses are expected in the gamma range.

The gamma light curve³ detected by Fermi shows one very interesting feature of critical importance to this project. The pulses show a significant broadening from the radio to the gamma range, by a factor of around 6-7, as shown in Figure 4. It is unclear if this same broadening will occur to the length of the giant pulses, as there is no data on gamma giant pulses. For this project, it will be assumed that the broadening applies to both ordinary and giant pulses, i.e. that the broadening is caused either by a part of the production mechanism that is common to both types of pulse, or by a factor external to the production mechanism, for the principal analysis. In addition to the principal results, the observational results for 'short' duration giant pulses will be examined, and any differences discussed.

³ The terms light curve and pulse profile both mean the same, namely a histogram of the count of photons per phase bin. Both terms will be used interchangeably in this report.

1.6 The Vela Pulsar

The Vela Pulsar is the brightest source in the gamma-ray sky, (12) and as a consequence is often used as a standard candle by new telescopes. Its inclusion in the project is to give a baseline of performance of the various telescopes, to allow for comparison with currently available telescopes. It has a period of 89.32 ms (18), and is located approximately 290 parsecs (18) from the Earth. It is much older than the Crab, at 11 300 years old. (18) Due to its location in the southern hemisphere, the Vela Pulsar will be a key target for the CTA South array, both for research purposes, and as a calibration and performance test for the array. The Vela also exhibits behaviours known as giant micro-pulsing (19), and timing glitches, where the pulsar randomly speeds up for a period, the mechanisms of which are not understood.

1.7 Giant Pulses

The primary goal of this project is to assess whether the new arrays will be capable of resolving or detecting giant pulses. These phenomena are one of the most intriguing and enigmatic features of pulsars, and have been detected in several pulsars, (20) including the Crab. They are characterised as a short duration pulse of extremely high intensity. A giant pulse is characterised by an average intensity greater than 10 times that of the mean pulse intensity. (19)

Several studies of giant pulses in the Crab have been performed in the radio range, which have given fairly consistent results. Giant pulses seem to occur approximately every 5-6 minutes (21)⁴, and the magnitudes of the giant pulses follow either a power law or broken power law distribution (17). In the case of the Crab, these power laws have indices which appear to have some dependence on frequency (17), but fall within a range, in the case of a single power law, from -2.2 to -2.9. (17) With a broken power law, the indices vary from around -1.0 to -1.9 in the low energy regime, and -1.7 to -3.2 in the high energy regime. (17) An interesting feature to note is that the duration of a giant pulse appears to have some correlation to its magnitude, with the most intense giant pulses being of shorter duration. (17)

A further area of interest is the confusingly named giant micro-pulses seen in the Vela. As well as presumably being a strong contender for the Most Contradictory Name in Science award, these phenomena that have been observed in the Vela pulsar in the radio range, where a small section of the pulse profile, just leading the main pulse (19), can be randomly boosted, achieving peak intensities greater than ten times the mean intensity of the pulsar. (19) These phenomena are differentiated from giant pulses in that their mean intensity does not exceed the mean pulse intensity by a large margin. (19) The relationship between the giant micro-pulses and the Giant Pulses of the type observed in the Crab is not clear, if indeed there is any relationship at all.

⁴ A recent release on arXiv gives a much higher rate, of approximately 1.1 Hz in the P1 pulse, 0.17 Hz in the P2 pulse (25). This paper concentrated on looking for lower magnitude giant pulses, which may explain the large increase in the event rate.

2.0 Preliminary Work: Detection and Background Rates

Before a model of the pulsar itself is written, it is essential to know how well the various instruments will function. This involves calculating the rate at which they will detect photons from a source and estimating the rate at which background photons will be detected. For a point source like the Crab and Vela pulsars, only the background within one field of view of the telescopes must be considered, simplifying the calculations considerably. The results of these calculations are the groundwork for the remainder of the project. The method for calculating the background and detection rates will be described, the results given and discussed. Some additional rates will also be calculated, to allow proper comparison of the new instruments with their current counterparts.

2.1 Method for Calculating the Detection Rate

To calculate the rate at which photons will be detected from a source by an instrument, two pieces of information are needed; firstly the energy spectrum produced by the target, in the form of a differential flux by area and energy, and the effective area of the instrument as a function of energy.

The spectrum for an object must be deduced from theory, if the source has never been observed before or if a new energy range for a particular source is being observed, or if, as in this case, instruments already exist that can observe the phenomena, from observational data. In the case of these pulsars, instruments, especially space based satellite telescopes, have provided us with different spectra we can use.

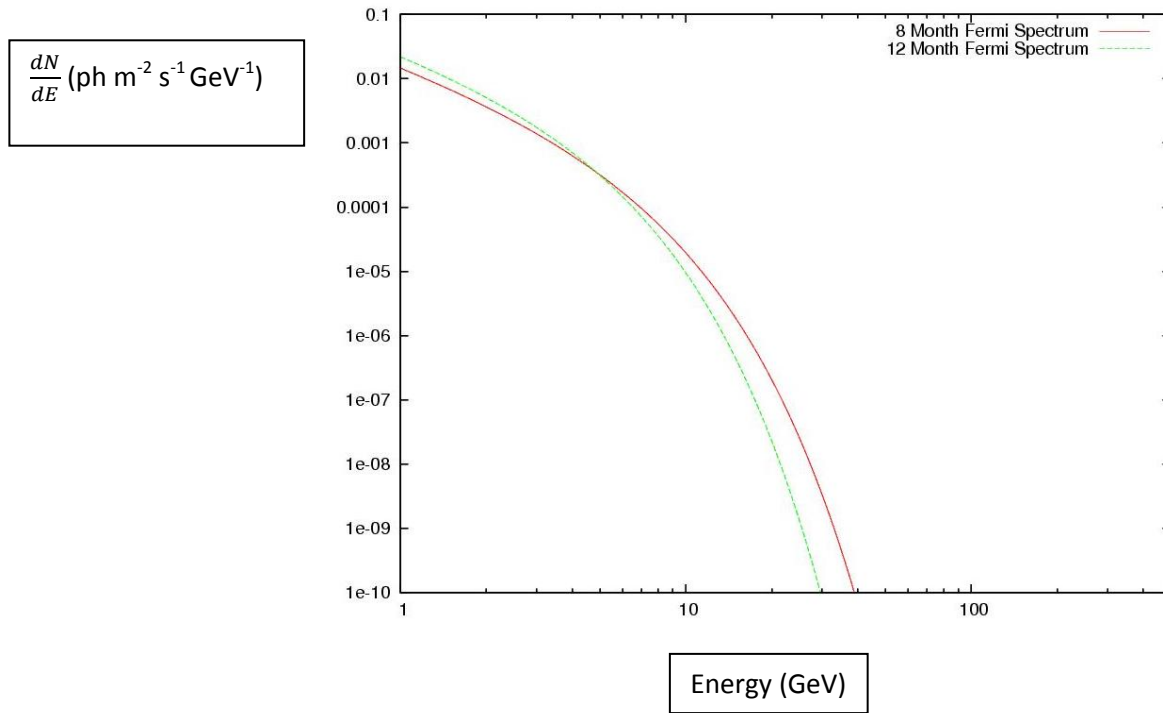
Determining the effective area of the telescope as a function of energy is usually done by performing simulations of the instrument, an example of the methodology for this is described in Aharonian et al 2001 (14). In the case of an array, as well as testing the performance of the equipment itself, simulations are often performed in order to optimise the layout of the array, i.e. what number of telescopes there should be, how widely they should be spaced, how many of different sizes there should be, for the physics goals of the instrument.

In the case of the Vela pulsar, the most current spectral data available comes from the Fermi space satellite, using the Large Area Telescope. Two papers have been produced, one using the first eight months of data, one using the first year of data, each of which gives a different spectrum for the Vela. The first spectrum is a standard power law with exponential cut-off, show below in Figure 5.

The second paper gives a spectrum with a sub-exponential cut-off, shown in Figure 5, where the argument of the exponential function is raised to a power smaller than one. This results in a slower drop off in the spectrum, which would increase the detection rate, as the pulsar emits more of its power in the energy range where the telescopes have larger effective areas, if the cut-off energy was equal. In this case, however, the cut-off energy also falls, reducing the detection rate of the pulsar.

Figure 5: Spectra for the Vela Pulsar from the Fermi LAT

The two spectra for the Vela pulsar as derived from the Fermi LAT observations. The slower decay of the 12 month spectrum can be seen, although the lower cut-off energy causes the spectrum to attenuate faster. In comparison to Figure 6 below, it can be seen that the normalisation of the Vela spectrum is higher than for the Crab, but that the energy cut-off is lower.



For the Crab, there are four available spectra from the most advanced instruments. The Fermi spacecraft provides a spectrum, a power law with an exponential cut-off. In addition, the MAGIC ground based IACT array has the ability to detect the Crab, and gives a series of possible spectral fits, one with an exponential cut-off, and two with super-exponential cut-offs, one using a fixed index of 2, and the other leaving the index as a free parameter. It is indicated in the paper that the fit with the index left as a free parameter is regarded as the best fit (5), so it shall be used as the standard MAGIC spectrum for the purposes of this project. The Fermi spectrum and the MAGIC spectrum which will be used are shown below in Figure 6.

Two further spectra for the Crab will also be examined, though both should be viewed as best case scenarios in some respects. The first will be the Fermi spectrum's normalisation and power law, but using the MAGIC cut-off energy from the exponential cut-off, shown in Figure 8. As Fermi cannot extend its observations to as high an energy as MAGIC can, it is plausible that the Fermi spectrum underestimates the cut-off energy. As can be seen in Figure 7, the MAGIC data points do indicate a substantial deviation from the proposed Fermi trend. At the same time, the MAGIC telescope's range does not extend to the lower energies covered by Fermi, so it is plausible that the Fermi parameterisation is more valid in this range.

Figure 6: Fermi and MAGIC spectra for the Crab Pulsar

This plot shows the differential flux of the Crab pulsar, as modelled by the Fermi and MAGIC collaborations using data from their observations. The higher normalisation of the Fermi spectrum is clearly visible, as is the extension of the energy range caused by the MAGIC spectrum's higher cut-off energy.

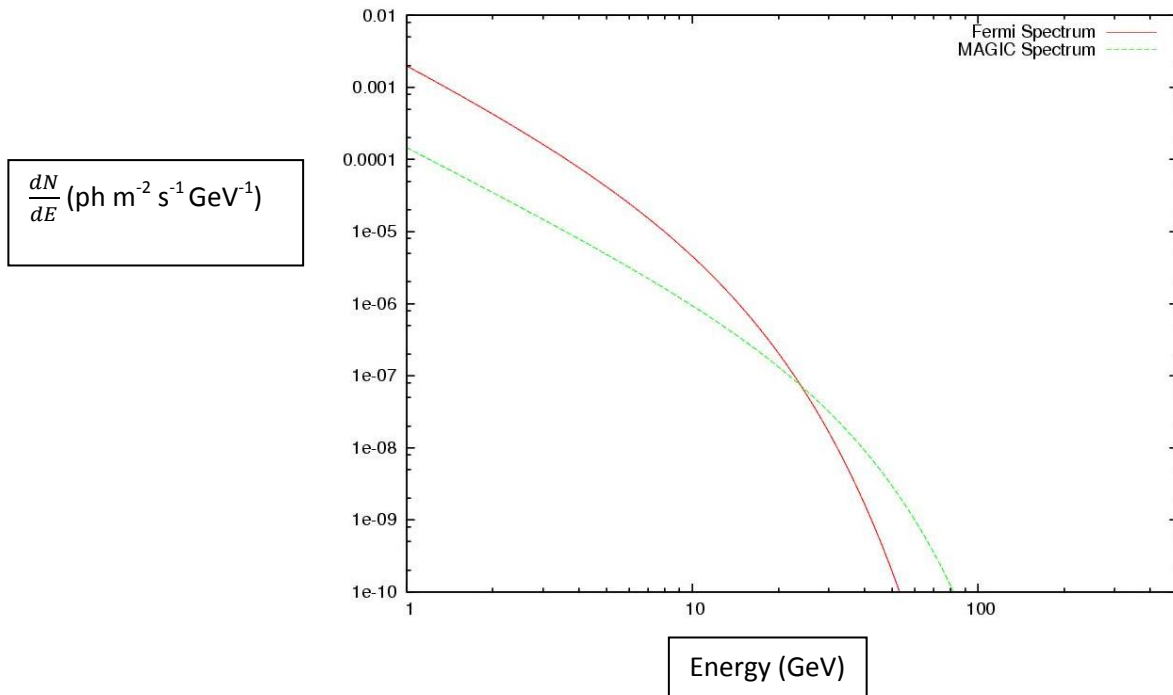
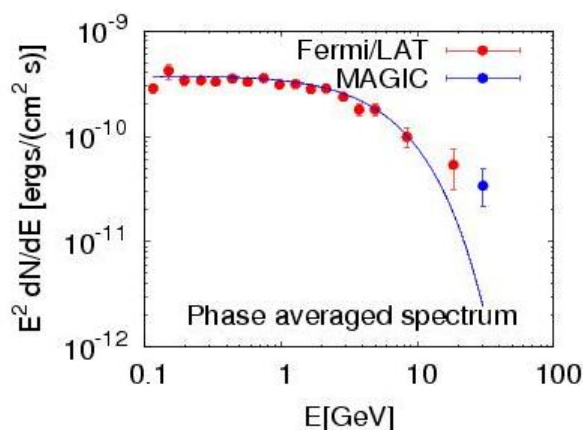


Figure 7: Plot of Fermi and Magic data points compared to the Fermi spectrum

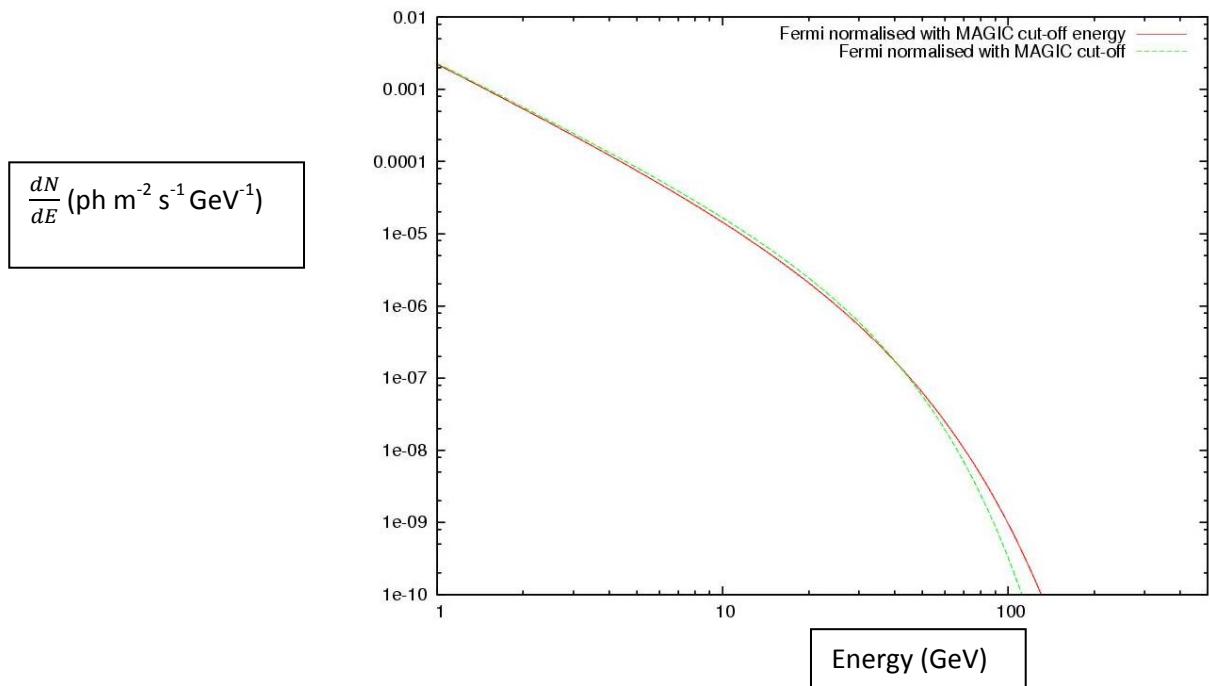
This plot shows the Fermi spectrum and compares it to the data points recorded by the MAGIC and Fermi LAT telescopes. The deviation from the Fermi spectrum recorded by MAGIC is clear.



The second 'hybrid' spectrum, shown in Figure 8, uses the Fermi normalisation and power law index again, but utilises the best fit MAGIC decay. The same arguments for the first hybrid spectrum again apply here, although it must be stressed that both of these spectra are not produced from observed data, and are based on the work of two different instruments with no cross referencing to confirm their compatibility. As such, systematic differences between the two instruments here could be distorting the results heavily.

Figure 8: Hybrid spectra for the Crab Pulsar

Here the two hybrid spectra, combining aspects of both the MAGIC and Fermi spectra, are shown. The difference between the two is small, but compared to the MAGIC or Fermi spectra, the differences are large.

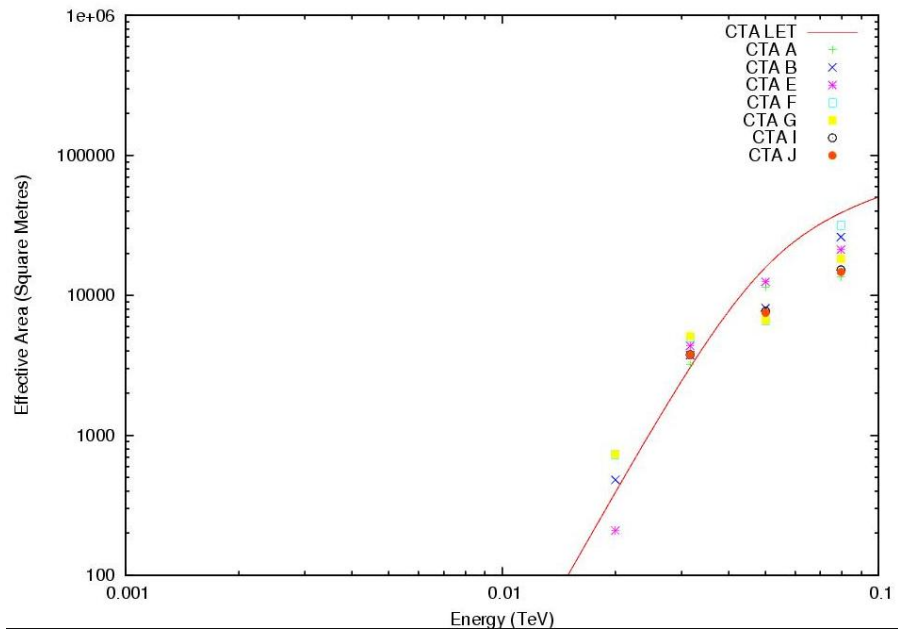


The effective area curve for 5@5 has been calculated from simulations by Aharonian et al. (14), and is shown in Figure 3. The simulations performed to arrive at this result are not as detailed or developed as those performed by the CTA collaboration on their array, nor has any attempt been made to optimise the layout of the telescopes (14), so the actual performance of a 5@5 type array could be somewhat different. To err on the side of the caution, it will be assumed that the results derived from the calculated rate represent a best case scenario for the 5@5.

For the CTA LET configuration, data was taken from the CTA Collaboration's Monte Carlo simulations for sub-arrays A, B, E, F and G (22). A curve was fitted to these data points which approximated the average behaviour of all the sub-arrays, as shown in Figure 9. The available estimates are for the post cut effective area, with the cut efficiency under ~ 300 GeV being very poor, at around 5-20%, as the cuts are optimised for high energy (around the TeV) energy ranges. With improvements to the selection cuts, the effective area could be massively improved, perhaps by a factor of 5 to 10. The selection cuts are designed to eliminate hadronic signals, but at the lower energies where pulsar emission is strong, the hadronic component of the background is extremely small, leaving only the photon and electron signals. Electron background can be limited by placing an instrument near the equator, where the Earth's magnetic field will provide a shield from the charged electrons. As such, the CTA LET estimate represents a worst case scenario for the CTA.

Figure 9: Fitting of the CTA LET curve to the CTA sub-array data points

The fitted curve and the raw data points from the CTA collaborations simulations over the energy range of the pulsar spectrum. It can be seen that the effective area is very low in the areas of strong pulsar emission, which limits the performance of the CTA with the selection cuts used in the simulations. Data points from CTA WP Prod Wikipage. (22)



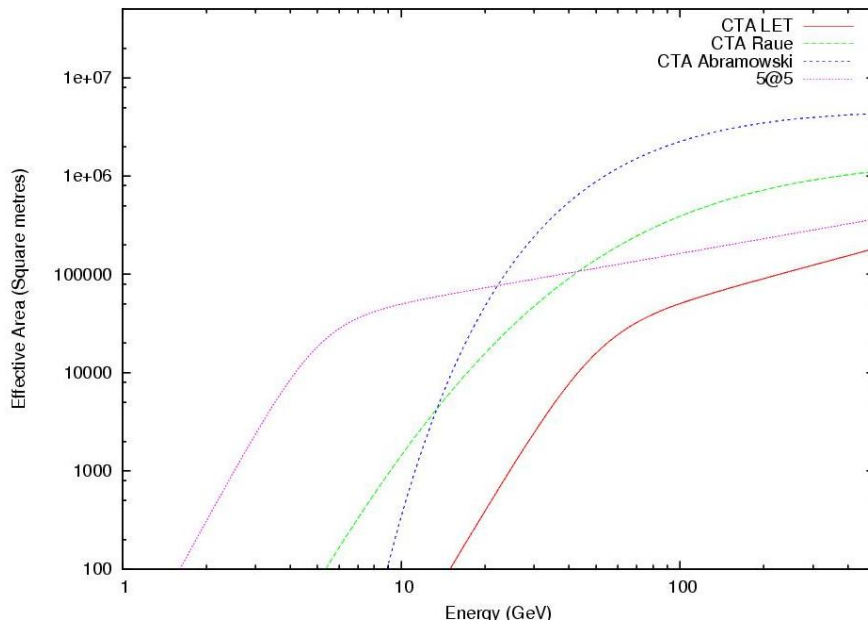
For the purposes of this project, given that the actual final design of the CTA has not yet been chosen, a more general approximation should give a better baseline for the expected performance of the array. When the layout of the array is finalised, and more detailed simulations have been performed, the analysis presented in this project could be utilised to achieve a more accurate assessment of the array’s actual capabilities.

Two further estimates of the CTA’s performance are also examined. Firstly, a curve from Abramowski et al 2010 (23), which uses the expected performance of H.E.S.S. Phase II as a grounding, scaling up the effective area with the size of array and shifting the energy threshold to a lower value to allow for the inclusion of the large diameter telescopes and dense central core expected in the CTA. This estimate, henceforth referred to as CTA Abramowski, is an optimistic view, with by far the largest effective area of any of the estimates. The results derived from this estimate should therefore be taken as best case results.

The final estimate, derived by Raue and Mazin 2010 (24), is based on the performance of the MAGIC telescope array with the sum trigger system. Again, the threshold has been reduced and the area has been scaled up with the expected array area of CTA. This estimate corresponds quite well to the estimated pre-cut effective area of the CTA LET arrays being simulated. This means that this estimate will provide a good idea of how the CTA may perform with efficient low energy cuts. All the effective area curves for the CTA and 5@5 are shown in Figure 10. From the plot it can be seen that the 5@5 effective area reaches higher values at the lower energy range, due to the positioning of the array, and that after a point the CTA curves overtake 5@5, due to their higher overall area and number of telescopes.

Figure 10: The Effective Area Estimates for CTA and 5@5

This plot compares all the estimates that will be used in this project. The advantage of a 5@5 type array at lower energies is apparent, and the limitation it faces from the actual size of the array at higher energies. The different energies where the CTA estimates become more effective observational tools than 5@5 can be seen at the intersection of the curves.



Using these curves, the detection rate can be calculated by folding the spectra with the effective area curves, and then integrating, normally numerically, over the energy range of observation. The energy range selected for this project was from 1 to 100 GeV. The lower limit was chosen to be lower than the energy threshold of any of the instruments, to ensure that all of the useful effective area of the arrays is counted in the calculations, and the upper limit was chosen to be at a level where the pulsar emission was minimal. A higher limit would not significantly improve the detection rates of the instruments, but would affect the background rate, adversely affecting the results collected.

2.2 Method for Calculating the Background Rate

The method for calculating the background rate for the arrays is somewhat different to the method used to determine the detection rates, as it requires the taking into account of multiple sources of contamination in the signal, from electrons to heavy nuclei, and analysis of how these signals will appear to the telescopes and array as a whole. A direct determination of these factors requires massive computing power and significant periods of time, placing it well beyond the scope of this project. In order to overcome this obstacle, a simplification will be used to exploit some available data.

The CTA Collaboration has performed Monte-Carlo simulations of the sub-arrays being investigated in order to determine the rate at which background events will be detected. These simulations have given the background rate for discrete energy ranges. The background rate for the CTA LET

configuration was calculated by summing these values, with appropriate weighting for the width of the energy bands, between 1 and 100 GeV, giving a background rate for the CTA LET.

This value was used to extrapolate background rates for CTA Abramowski and CTA Raue. The effective area curves of each telescope were folded with a simple model of the background radiation, a simple power law of index -2.7 without normalisation, and this curve was then integrated between 1 and 100 GeV. The CTA LET background rate was multiplied by the ratios between the integrated flux of the CTA Abramowski and CTA Raue estimates and the integrated flux of the CTA LET to give the background rates for the CTA Abramowski and CTA Raue estimates.

This method for calculating the background rates rests on the assumption that the performance of the telescopes and arrays in each of the three estimates is more or less identical, and that the scaling effects of increasing the effective area are minimal. The effective area of an IACT array can be, at a simplified level, taken as the area of the array itself plus a band with the width of a Cherenkov radius around the edge. For a small array, such as 5@5, this band is a significant addition, contributing a significant fraction of the effective area. The proportion which the band contributes varies rapidly with changing side length at first, with the variation decreasing with increasing side length. For example, at 900 metre side length, the band forms 33% of the effective area, at 1000 metres it forms 31%. For very large arrays, such as the CTA, the proportion will remain fairly consistent, so the scaling of the background will not be adversely affected by changes in this band.

The assumption that the telescopes and array will function in a very similar manner is more difficult to justify. Neither the CTA Abramowski or CTA Raue estimate are based on simulations of arrays, but based on the performance of current telescopes (H.E.S.S. and MAGIC respectively), so provide no data on triggering etc that can be used as a comparison with the CTA collaborations simulated array. On the other hand, the fact that neither provides details gives carte blanche for the assumption that the different arrays are using the same operational parameters. Also, the CTA's operational parameters will be based at least in part on current IACTs, of which MAGIC and H.E.S.S. are two of the most successful. This assumption, although potentially open to question, allows for producing a background rate without the need for detailed simulations, which are beyond the scope of the project and resources available.

The 2001 Aharonian paper provides differential background rates for electrons, protons and photons. Assuming the 5@5 array will be built away from the poles, the geo-magnetic cut off should be very high, allowing all electrons to be ignored in the energy range relevant for pulsar observations, and stereoscopic imaging allows for the rejection of most hadronic showers, meaning that the proton background can also be largely neglected. Integrating the photonic background over the energy range of 1 – 100 GeV gives the final background rate for 5@5.

2.3 Results: Detection Rates

Using the method described in Section 2.1, and the spectra and effective area curves presented there, the detection rates for each instrument/spectra combination was calculated, using

Mathematica v 6.0 for the numerical integration. Using the errors in the parameters of the spectra, both statistical and systematic, errors on the estimate were calculated, taking the shallowest power law, highest cut off energy and highest normalisation for the maximum detection rate, and the lowest cut off energy, lowest normalisation and steepest power law for the lowest detection rate. The results of this are tabulated below in Table 1.

Table 1: Photon Detection Rates for 5@5 and CTA

| Gamma Photon Detection Rate (Hz) in the range 1-100 GeV | | | | | |
|--|--|--|---|--|----------------------------|
| Pulsar | Spectrum | CTA LET | CTA Abramowski | CTA Raue | 5@5 |
| Vela | 6 month Fermi Spectrum | $3.79^{+2.50}_{-1.54} \times 10^{-3}$ | $1.88^{+1.66}_{-0.92} \times 10^{-1}$ | $3.27^{+1.84}_{-1.21} \times 10^{-1}$ | $30.48^{+11.34}_{-8.59}$ |
| | 1 Year Fermi Spectrum | $1.78^{+26.77}_{-1.65} \times 10^{-3}$ | $4.19^{+188.80}_{-4.14} \times 10^{-2}$ | $1.89^{+18.62}_{-1.72} \times 10^{-1}$ | $27.58^{+105.28}_{-23.33}$ |
| Crab | Fermi Spectrum | $2.03^{+3.24}_{-1.39} \times 10^{-3}$ | $1.70^{+2.92}_{-1.24} \times 10^{-1}$ | $1.05^{+1.13}_{-0.62} \times 10^{-1}$ | $4.83^{+2.46}_{-1.93}$ |
| | MAGIC Spectrum | $1.73^{+1.10}_{-0.95} \times 10^{-2}$ | $1.05^{+0.57}_{-0.53}$ | $2.14^{+1.04}_{-0.98} \times 10^{-1}$ | $1.11^{+0.26}_{-0.21}$ |
| | Fermi spectrum with MAGIC cut-off energy | $5.98^{+9.03}_{-4.35} \times 10^{-2}$ | $4.48^{+5.87}_{-3.12}$ | $1.13^{+1.20}_{-0.70}$ | $12.91^{+5.57}_{-4.77}$ |
| | Fermi spectrum with MAGIC exponential term | $3.36^{+3.79}_{-2.19} \times 10^{-1}$ | $20.30^{+20.11}_{-12.43}$ | $4.07^{+3.71}_{-2.34}$ | $19.79^{+7.56}_{-6.40}$ |

The first point that is obvious from these results is that the fit of the spectrum is of critical importance to determining the performance of the instruments. The large errors in the parameterisations of the curves translate into massive errors in the detection rates, making definitive statements on the performance of the arrays challenging.

The most critical parameter for determining the detection rate in most cases is the cut-off energy of the pulsar. As can be seen in the case of the Crab, when the cut-off energy is increased, i.e. the MAGIC spectrum or hybrid spectra are used, the rate of detections increases massively for all of the CTA estimates. One slight aberration in this trend is the 5@5 detection rate for the MAGIC spectrum, which is actually lower than the Fermi spectrum rate. This can be explained as the normalisation of the MAGIC spectrum is approximately an order of magnitude lower than the Fermi normalisation. This can be explained by looking at 5@5's effective area curve. As the curve flattens off at a low energy, the gain in effective area for each unit increase in energy is small beyond around 8 GeV. This coupled with the low normalisation of the pure MAGIC spectrum restricts the rate for 5@5. It can be

clearly seen from the hybrid spectra, however, that when this normalisation is kept constant, increasing the cut-off energy again radically increases the detection rate.

For comparison, the detection rates for MAGIC and Fermi's LAT were calculated, as shown below in Table 2. For the LAT a very simple effective area (a constant of 0.8m^2) was taken, whereas for MAGIC an effective area curve was fitted to the data published in Aliu et al. (5). The methods used to calculate the detection rates were identical to those described above.

Table 2: Detection Rates for Fermi's LAT and MAGIC

| Detection Rates (Hz) for the Fermi LAT and MAGIC with different spectra | | | |
|--|--------------------------------|-----------------------|-----------------------|
| Pulsar | Spectrum | Fermi LAT | MAGIC |
| Crab | Fermi | 1.17×10^{-3} | 8.85×10^{-4} |
| | MAGIC | 1.06×10^{-4} | 4.79×10^{-3} |
| | Fermi normalised MAGIC cut-off | 1.57×10^{-3} | 1.74×10^{-2} |
| | Fermi normalised MAGIC decay | 1.75×10^{-3} | 9.30×10^{-2} |
| Vela | Fermi 8 months | 9.34×10^{-3} | 1.99×10^{-3} |
| | Fermi 12 months | 1.28×10^{-2} | 9.56×10^{-4} |

2.4 Results: Background Rates

Using the method described in Section 2.2, and the effective area curves shown in Section 2.1, background rates were calculated for the instruments under investigation, and are presented here in Table 3. These results are independent of the spectra being examined.

Table 3: Background Rates for each Instrument in the range 1 to 100 GeV

| Telescope | Background Photon Detection Rate (Hz) per field of view |
|----------------|---|
| CTA LET | 0.20 |
| CTA Abramowski | 3.43 |
| CTA Raue | 0.96 |
| 5@5 | 12.34 |

2.5 Discussion

As can be clearly seen, in many cases the background rates far exceed the expected detection rates, especially in the case of the conservative Fermi and MAGIC spectra. This will limit the ability of the arrays to detect short lived phenomena, as the random noise will obscure all but the strongest of signals. The high noise should not, however, affect the pulse profiles too strongly, as over a long enough period of observation, which will vary from instrument to instrument, the background count in each phase bin should be approximately equal, meaning any significant variation will be due to the pulsed emission above this.

In the case of the Crab, none of the detection rates are high enough to allow the resolution of individual pulses, as no rate is equal to or greater than the frequency of the pulsar (~ 30 Hz for the Crab). For the Vela, the CTA detection rates are also too low to allow for the resolving of individual pulses, however 5@5's detection rate of around 30 Hz is greater than the frequency of the Vela (which is ~ 11 Hz), meaning that around two to three photons should be seen per pulse. Although the data will be sparse, this represents the possibility of actually resolving individual pulses. Also, this high rate of data collection will allow the building of detailed pulse profiles in very short observation periods, potentially allowing for the study of evolution of the pulse morphology and period in the gamma range. In addition, it may be possible to study if glitches occur in the gamma range, if the glitches last long enough.

3.0 Method: Modelling the Crab Pulsar

Of the two pulsars selected for close examination, the Crab displays the most interesting phenomena, namely giant pulses, with the added bonus that these phenomena are both well studied, if not well understood, and very energetic, making detection more likely. Consequently, it was decided to model the Crab, even though it will be at the limit of the CTA South's observational field, as the Crab is a northern hemisphere object.

3.1 Structure of the Model

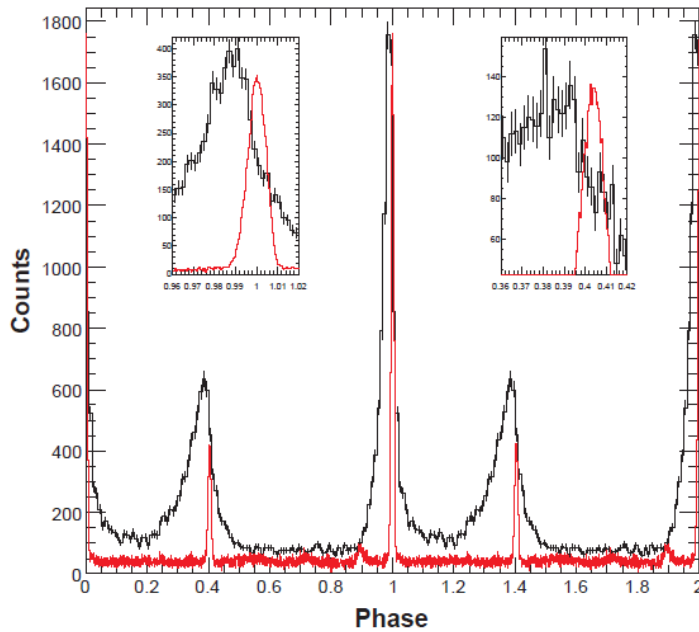
To reproduce the observations of the arrays, a computer model of the Crab and array will be written, which will give out photons from the pulsar's standard pulses at a rate suitable for the array being simulated. In addition to these 'signal' photons, the model will incorporate a background, again, suitable to the array being simulated. In order to allow the program to be applied to all the telescope and spectra combinations, the detection rate and background rates will be user inputted variables. The model will also generate giant pulses, which will occur randomly, with random magnitudes. From these giant pulse events, it will calculate the number of photons that will be detected from each pulse. To ensure reproducibility, and to allow multiple simulations of the same type with different results, the user will be able to input a seed number for the random sequence, with 1 being the standard starting value.

Each photon generated will be assigned an arrival time through the observation period and a phase. For the signal and giant pulse photons, the phase will follow the Fermi light curve for the Crab, shown below in Figure 11, and for the background photons the phase will be randomly selected across a cycle. It should be noted that although the MAGIC light curve covers an energy range similar to the energy range that will be observed by the CTA and 5@5, thus in many ways making it a more suitable curve to follow in the model, the data available from the MAGIC telescope is far more sparse than that of Fermi, which would limit the accuracy of reconstruction. Also, the far less developed view of the light curve may well prevent analysis of the level of features which could be resolved by the new arrays. In addition to the raw data for each photon, the program will also output a light curve histogram, recording the count of photons arriving in each phase bin for the entire observation period.

Figure 12 shows a flow chart representing the structure of the program. The most critical, in some respects, part of the program is the phase assignment for each photon. As the only tool available was the C++ random number generator, which has a uniform probability distribution, a method of converting this to a non-linear probability distribution had to be used, specifically following the Fermi pulse profile. To do this, the count for each phase bin was read off the graph, and converted to a continuous distribution function. This was used to create a conversion table, with a number of entries equal to the count in a phase bin being assigned that phase. This allows for the creation of a random number between 1 and 22617 (the total number of photons in the pulse profile) by a linear generator, such as that available in C++, which can then be converted to reproduce the desired pulse profile.

Figure 11: The Pulse Profile of the Crab Pulsar above 100 MeV

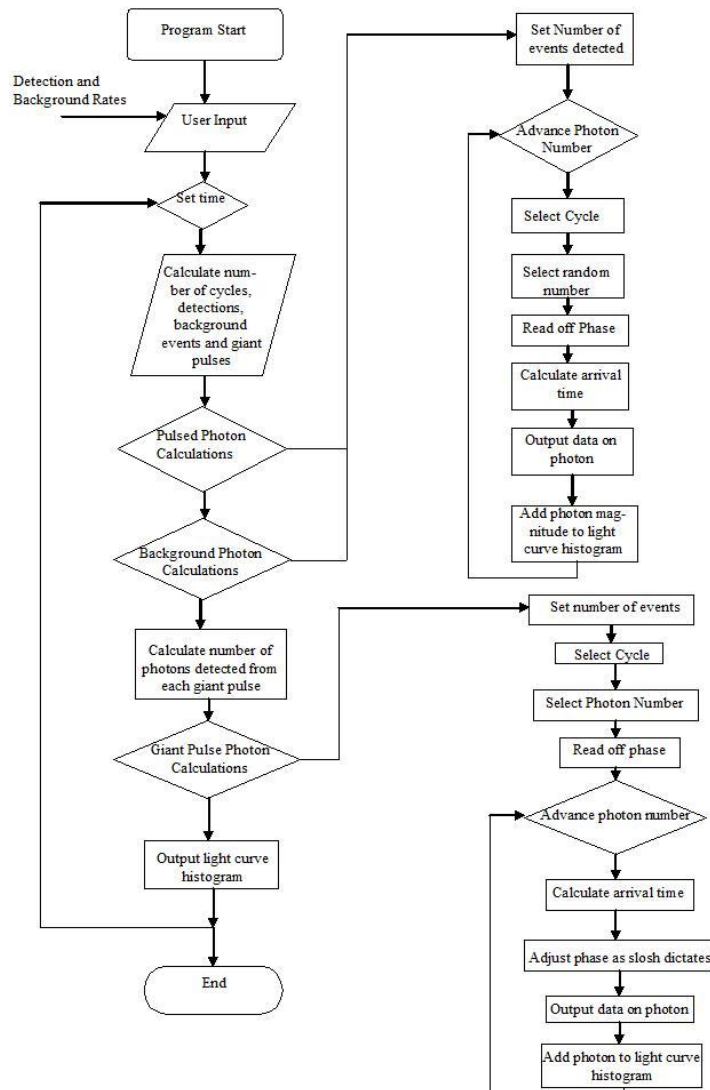
This graph shows the count of photons per phase bin recorded by the Fermi LAT telescope (the black histogram). The graph covers two full cycles. The inserts show details of the two peaks, and the red line shows the radio pulse profile. Image from FERMI LARGE AREA TELESCOPE OBSERVATIONS OF THE CRAB PULSAR AND NEBULA The Astrophysical Journal, Volume 708, Issue 2, pp. 1254-1267 (2010).



Each photon is assigned an arrival time, which is determined by randomly selecting a cycle of the pulsar (a cycle being one full period of rotation, 33.08 ms) through the observation period and multiplying the number of the cycle by the length of a cycle. Each pulsed photon is then assigned a phase, in the manner described above, following the Fermi pulse profile, and this phase multiplied by the period length is added to the time of arrival, giving an arrival time during the complete cycle. Further to this a random “slosh” is added to each photon, within the duration of the phase bin. This slosh uses the liner random number generator to choose a point through the phase bin with a uniform probability for each point. For background photons, the phase is assigned using a uniform probability distribution, as there should be no inherent bias to when the background photons arrive. Otherwise, the time assignment procedure is identical to that used for the pulsed photons.

Figure 12: Flow Chart of the Main Program

The structure of the program is represented here, showing the main body and the two calculation routines, one for the single photon events (background and pulsed photons) and the other for the multi-photon events (giant pulses). In the program written, the times were set to 0.5, 5 and 50 hours in the three loops.



3.2 Simplifications and Assumptions

The model developed has several major simplifications and assumptions built into it. Perhaps most crucially, particularly for the interval analysis, the giant pulses are assumed to have a rectilinear form, instantly reaching peak intensity and staying there for the duration of the pulse, when they instantly vanish. This means that the photons detected during a giant pulse have an equal chance of arriving in any unit of time during the giant pulse, whereas in reality, the pulses will have a form,

probably Gaussian, which would affect the distribution of the photons, making it more likely a photon would be detected in the centre of the giant pulse. This would reduce the interval between the arrival times of the photons, and give a more distinct spike in the results of Statistical Interval Analysis, the method for which is described in Section 3.5.

Further to this, it is assumed that there is no temporal pattern to the occurrence of giant pulses. The giant pulses in the model occur randomly with a frequency of approximately 3 mHz, equivalent to one every 5-6 minutes. The phases at which the giant pulses occur, however, is tied to the pulse profile of the Crab, as detected by Fermi. This means that giant pulses are more likely to occur in the P1 and P2 peaks than at other phases, as is indicated by the data. (17) Whether the giant pulses follow the light curve distribution so closely in reality is an open question. Technical aspects of the instruments are also ignored for simplicity's sake. Specifically, the dead-time, the time when the array is unable to take new data, is ignored.

The model is further simplified by neglecting the changing morphology of the pulse profile in different energy bands. As shown in Figure 4, the proportion of the P1 and P2 peaks changes with increasing energy, until they are almost equal in the highest observed energy band. The model does not take this into account, only using the Fermi light curve for all photons that are generated.

The calculation of how many photons are detected during a giant pulse is also simplified, taking no account of the duration of the pulse. In the model, the number of photons detected is calculated by dividing the detection rate by 30, to get the number of photons detected in an average pulse, multiplied by the magnitude of the giant pulse, i.e. how many times larger than an average pulse it is. An alternative option would have been to multiply the detection rate by the length of the giant pulse multiplied by the magnitude. This method would require additional components to the generation of the magnitudes of the giant pulses to be a totally accurate portrayal of the real giant pulses, as shorter pulses tend to be more intense (17).

3.3 Giant Pulse Simulator

The giant pulse simulation is a key point of the simulation, as the primary goal of the project is to determine if these phenomena will be visible. The following aspects of giant pulses are required to do this, firstly the magnitude of the pulse, meaning how many times brighter than an average pulse it is, referred to in this work as the boost factor, the number of photons that will be detected from the giant pulse, which depends on the boost factor and the sensitivity of the instrument, and the time and phase at which the giant pulse occurs. As a simplification, the simulator will work with a single power law distribution of the magnitudes, rather than a broken power law, of index -2.4, as a rough average of the detected results in the radio range. Although somewhat arbitrary, this choice seems to be the rough mean of observations taken at different frequencies, and as there is no current data on gamma ray giant pulses, we cannot know how the shift to gamma frequencies will affect the distribution, making any distribution ultimately an inference and subject to question.

The time and phase of a giant pulse as a collective entity was assigned in the same manner as that for a standard pulsed photon, described in Section 3.1. As a simplification, and as no pulse profile for

giant pulse occurrence seems to exist, the giant pulses are assumed to have the same probability distribution as the photons themselves, following the observation, described in Section 1.7, that giant pulses are more common in the P1 and P2 peaks. The individual photons detected during the giant pulse were each assigned a time stamp of their own. A random slosh of up to half the maximum giant pulse duration either before or after the giant pulse time was added to the timestamp of each photon. If the slosh was large enough, the phase of the photon was altered appropriately for the purposes of reconstructing the light curve.

To generate the magnitudes of the giant pulses, the linear random number generator must again be converted into a non-linear output, in this case a simple power law distribution. As the power law is a well defined function, unlike the pulse profile, an equation can be developed to produce the distribution, rather than a conversion table. Using the generated magnitude, the number of photons detected by the instrument in the giant pulse can be calculated using Equation 2. This equation simply takes the average number of photons detected in a pulse, simplified to the detection rate per second divided by 30 (the approximate number of pulses per second), multiplied by the magnitude of the giant pulse.

Equation 2: Photon Detection Count

$$\text{Number of photons detected} = \frac{\text{Rate of detection} \times \text{Magnitude of giant pulse}}{30}$$

3.4 Direct Observations

Ideally, it would be desirable that the arrays could directly resolve giant pulses. Giant pulses would be seen as a cluster of photons in a very short period of time. In the case that giant pulses are stretched in a similar manner to the main pulses this time frame would be of order 1.3 milliseconds, otherwise it would be of order 200 microseconds. The background to this signal would be the number of events where sufficient background and pulsed photons arrive in the same time period to equal the limit defined as a giant pulse.

To determine whether direct observation would be feasible or not, the expected number of each type of event must be calculated. For giant pulses this is a fairly simple procedure. Firstly the number of giant pulses within the observation period, for the purposes of the calculation the observation period will be set at 50 hours, must be calculated by multiplying with the frequency (set at 3 mHz in this project). Then, for each telescope/spectrum combination the minimum magnitude required to achieve the threshold number of photons must be determined by reversing the detection calculator shown in Equation 2 to give the boost. The probability of this magnitude or higher occurring can be calculated using Equation 3, shown below. Multiplying by the expected number of giant pulses in the observation time gives the expected number of detections. Equation 3 was derived by integrating the power law distribution of the magnitudes from the observed value M_{obs} to the maximum boost obtainable (2500).

Equation 3: Magnitude Probability Calculator

$$\text{Probability of Magnitude greater than } M_{obs} = -\frac{1.40002}{1.4} (2500^{-1.4} - M_{obs}^{-1.4})$$

For each section of the pulse, namely the P1 and P2 peaks and the inter-pulse regions, the proportion of giant pulses that would occur was determined approximately by determining the proportion of the photon detections in each region from the Fermi light curve, as shown in Table 3. The expected number over the whole period was divided accordingly between the results for each of the sections.

Table 4: Defined regions of the pulse and proportions of giant pulses that occur in them

| Section | Phase region | Proportion of Giant Pulses |
|------------------|---------------------|-----------------------------------|
| P1 | 0.92-0.05 | 17.8% |
| P2 | 0.30-0.45 | 58.0% |
| IP (Inter-Pulse) | Remainder | 24.2% |

For the background events, the procedure is slightly different. Using the detection rate and the background rate summed together, the average number of photons arriving in each 4 phase bin block can be calculated. For the P1 and P2 sections, the detection rate was boosted by an approximate scale based on the increase in photon count over the normal (inter-pulse) level. Using this mean value, a Poisson distribution can be used to determine the probability of n photons arriving in a block, where n is the value defined as the minimum count required for a signal to qualify as a giant pulse. Multiplying this value by the number of 4 phase bin blocks in the observation period, namely the number of phase bins minus three, multiplied by the proportion of the pulse for each region gives the expected number of coincidental detections of the signal by region.

It should be noted, that this method only calculates the number that cause exactly the threshold value of photons to be detected, not greater magnitude, so the numbers calculated represent a lower limit on the number of background events. As the Poisson distribution drops off very rapidly for very small mean values, as is the case here, each successive term is much less significant than the previous, meaning that the higher results can be neglected whilst retaining a reasonable degree of accuracy. Other errors, such as the parameterisations of the spectra will dominate far above this effect.

3.5 Variations to the Model: Statistical Interval Analysis

A second form of data output that is required, in addition to the light curves of the main program, is the interval between photon detections for Statistical Interval Analysis (SIA), which is an indirect method of observing giant pulses in the photon data collected. The advantage of SIA is that it can detect the presence of giant pulses, even if they cannot be directly imaged, or if the background of coincidence events obscures them. SIA looks at the intervals between photon detections in order to detect any patterns or anomalies to expected behaviour. In the case of the background and pulsed photons, which are detected at a steady, fixed rate, we would expect an exponentially decaying distribution of interval times, the decay constant of which would be related to the rate of detection. If the intervals chosen are short enough, then the decay would appear as a fairly even, or linearly falling distribution, as the time over which the analysis outputs data would not be a significant fraction of the decay time.

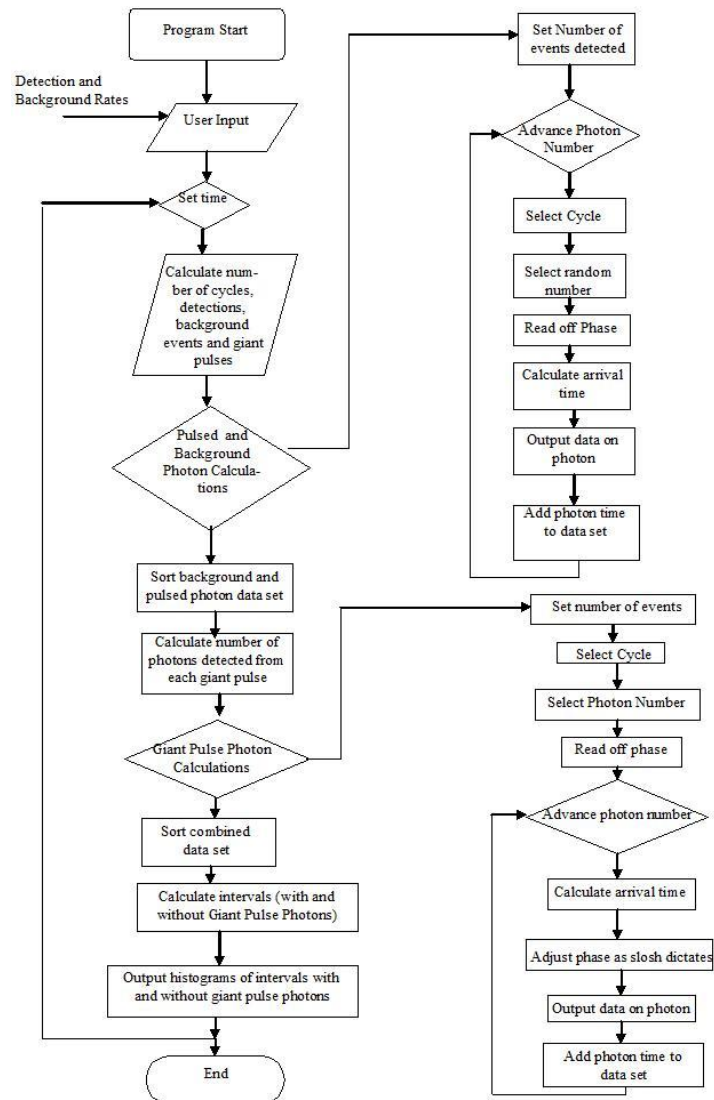
Giant pulses, on the other hand, although occurring at a fixed frequency, can be characterised by several photons arriving within a very narrow time frame, at most around 4 phase bins, or 1.3 milliseconds. This will give an abundance of very short interval times, which will show up above the exponential distribution of the signal and background photons, allowing for the identification of giant pulses. As the number of photons per giant pulse is not constant, the rate at which giant pulse photons are detected is not constant, thus will not form part of the exponential distribution.

To perform SIA, a restructuring of the program was required, principally in what data was outputted and how, and some additional data handling, specifically sorting the photons by arrival time. Figure 13 below shows a flow chart of the procedure for the Statistical Interval Analysis version of the program. One critical point here is that the sorting algorithm currently being used is a bubble sort algorithm. Although very reliable, it is an extremely slow algorithm for large data sets, which limits the observation times that are practical to simulate (depending on rate, the effective maximum can be anything from 50-200 hours). This represents in some ways a fundamental weakness in the program, but, as time on a telescope array such as the CTA or 5@5 will be fairly hard to acquire in large blocks, 50 hours of actual observations could represent months or even years of work, thus the limitation imposed here is probably not of tantamount importance to predicting observable phenomena. This technical point could and should be improved if this work is taken any further, but does not present any major obstacle to making predictions about the performance of these arrays.

In total 6 variants of the program were developed, 3 for producing light curves, 3 for producing interval analysis data. For both interval analysis and light curve simulation, two programs with set observation times of 0.5, 5 and 50 hours were produced, one with the expected maximum duration of giant pulses, and one with the short duration giant pulses (i.e. the same duration as radio giant pulses). For both interval analysis and light curve simulation there is a further program that allows the manual selection of both time and giant pulse duration, to allow more detailed examination of specific cases.

Figure 13: Flow chart of the structure of the SIA model

This flow chart depicts the structure of the program developed for the SIA. The sorting algorithm used was a bubble sort algorithm, but as it was included as a separate function called by the main program it could easily be replaced with a more efficient sorting algorithm.



3.6 Variations to the Model: Other Emission Modes

In addition to looking at the expected mode of emission, namely standard pulses with giant pulses, two further modes will be examined. Firstly, the standard emission mode but with short duration giant pulses, i.e. the broadening of the pulse seen in the radio and gamma light curves not applying to the giant pulses. To facilitate this, parameters defining the duration of giant pulses were altered in the code, leaving the flow of the program identical to the previous method.

The second, and more interesting, will assume that pulsed gamma photons are only created during the giant radio pulses. The justification behind this mode is that current detection methods can only detect photons at a lower rate than the rate of giant pulse occurrence, especially if the new data available indicating that giant pulses could occur at a rate of 1.1 Hz in the P1 pulse is correct (25). Two investigations will be made into this mode, firstly, what rate and average magnitudes of giant pulses could produce the observed results of the Fermi LAT experiment and secondly, what would be seen by the CTA and 5@5 under these conditions. Any potential signature of the two emission modes will be examined.

To allow the program to perform this simulation, the magnitude of detected event from pulsed photons was set to 0, meaning that no data would be recorded, even though the events themselves would still be calculated. This method was chosen in order to allow a fairer comparison with the data for the standard model, as an equal number of iterations would be performed if the conditions were set to be the same, meaning the same random numbers would be used for the giant pulse and background generation. This argument does not apply to the simulations where the background rate and magnitude of the giant pulses were altered. Two variants of the main program were written to perform this analysis, both with manual selection of observation times and giant pulse duration, with one outputting all data on the photons, and one only outputting the light curve histograms in order to avoid unreasonably large output files.

3.7 Testing of the Model

In the model, there are three key components which require testing. Firstly, the phase assignment for the pulsed photons (and giant pulses), the sorting algorithm for the photons (in the SIA versions of the model) and the magnitude generator for the giant pulses.

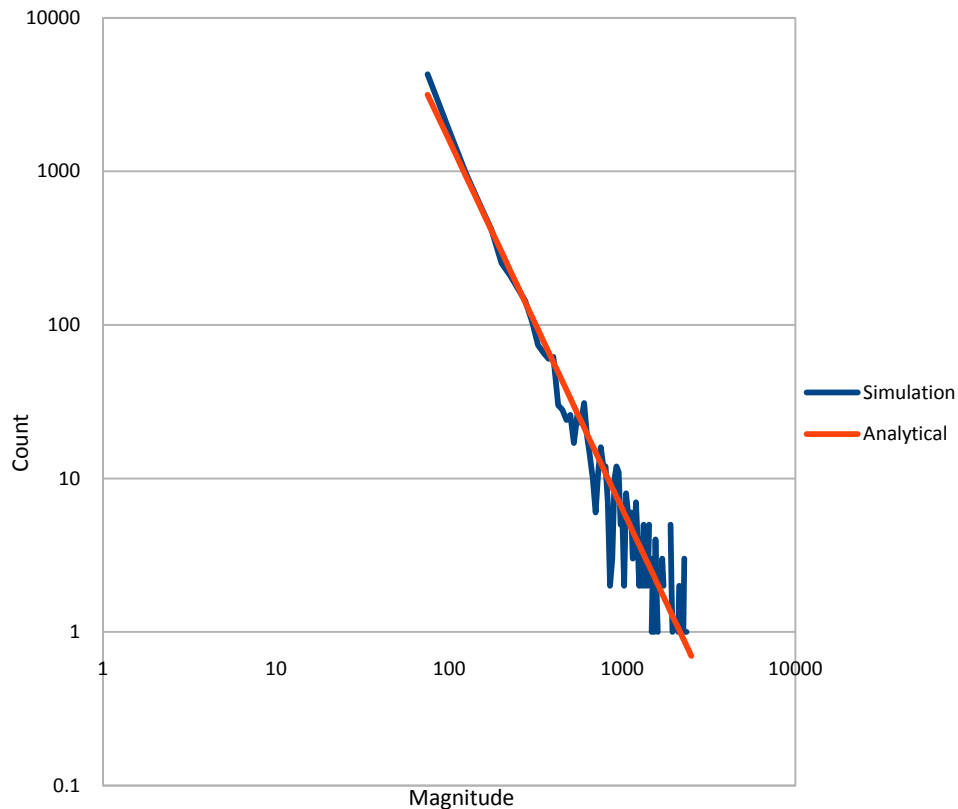
To test the sorting algorithm, the program was run on small data sets, with entries chosen to be challenging for the engine, such as very similar values and equal values. The lists were examined manually to determine if the algorithm had functioned. In all four tests performed, the list was correctly sorted, with no infinite loops triggered by the equal entries.

The phase assignment method was tested by running the model with only pulsed photons being included. The profile that emerged after a 100 hour observation period was compared to the Fermi pulse profile, and the deviations were analysed. No phase bins showed any major deviations from the pulse profile were seen, with the deviation in individual phase bins being of order 1% or less.

A test of the magnitude generator was run by writing a program to produce a histogram of the magnitudes produced. An analytical power law distribution was plotted alongside this data, as shown below in Figure 14, with a suitable normalisation. The two lines conform closely, until the very high magnitudes, where the statistics are too poor to allow for proper analysis.

Figure 14: The results of the tests of the giant pulse magnitude generator

The analytical distribution and the simulated distribution of the magnitudes are compared here. In the region where the generator gave a high number of results, the distributions match clearly. The tail end of the distribution is distorted by the low count of the results, allowing random noise to dominate.



4.0 Results

This section will detail a selection of the results from the simulations performed, arranged by the type of analysis that was being performed. In some cases, results from the simulations have been omitted if it was felt they were superfluous in combination with other results. For example, not all light curves simulated will be shown, as some either showed no useful data, or only increased the count on a shorter observation time result, rather than developing new features. Some additional results that have been omitted in this section have been included in the appendices on the attached CD.

4.1 Simulated Light Curves

Light curves were simulated for the three standard observation times (0.5, 5 and 50 hours) for each instrument/spectrum combination using the standard seed number for the random sequence. The plots here show the proportion of the count in each phase bin which is due to each of the sources of

photons (pulsed, background and giant pulse), to allow for clarification and analysis, though in the real results all that would be seen would be the total count per phase bin, as such distinctions would be impossible.

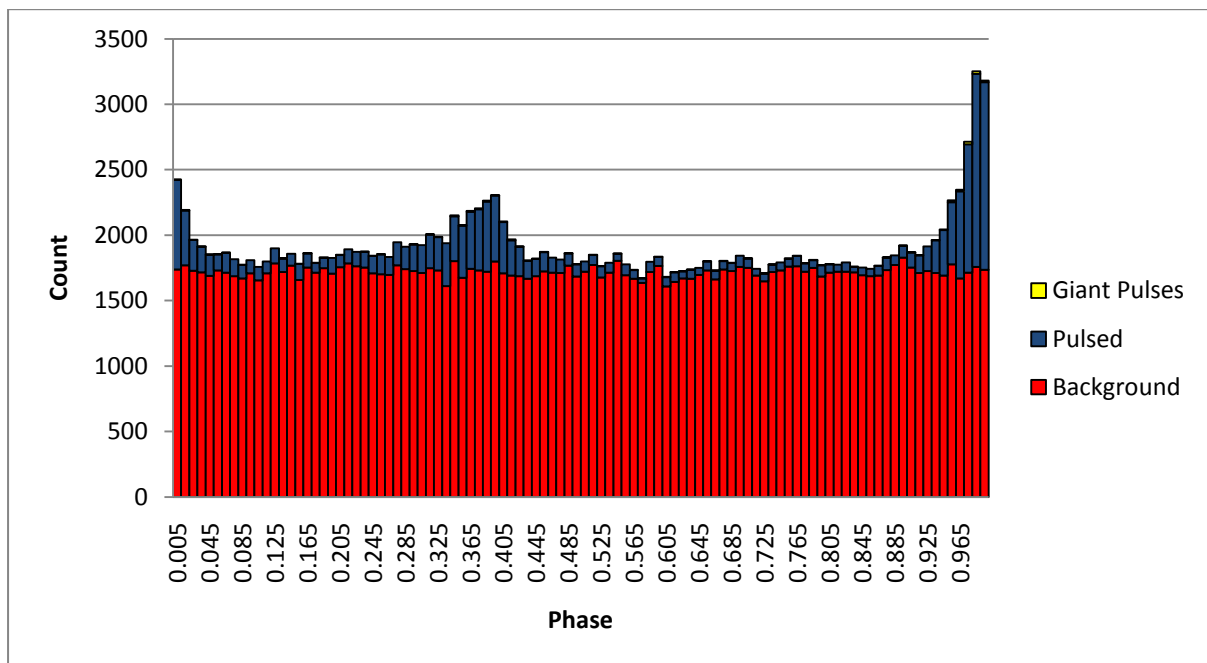
The simulated results for the CTA LET estimate show that for the two pure spectra no significant details of the pulse can be seen, even after 50 hours of observations. Variations in the background count between phase bins are far larger than the signal counts even for the P1 peak, obscuring the signal from the pulsar. In Appendix I Figure 1 the results for the Fermi spectrum are shown. The two hybrid spectra, however, produced far more promising results, allowing a good reconstruction of the pulse profile in less than 5 hours. Both the P1 and P2 peaks can be clearly identified in the pulse profiles, and some giant pulse photons contribute to the pulse profile, although not significantly. Appendix I Figure 2 shows the results for the Fermi normalised MAGIC decay spectrum with 0.5 hours of observations.

The CTA Raue estimate, which approximately represents the pre-cut effective area of the CTA, gives far more promising results, even for the Fermi spectrum. Presented here in Figure 15 are simulated light curves for all four different spectra, for the shortest observation time that gives clear results.

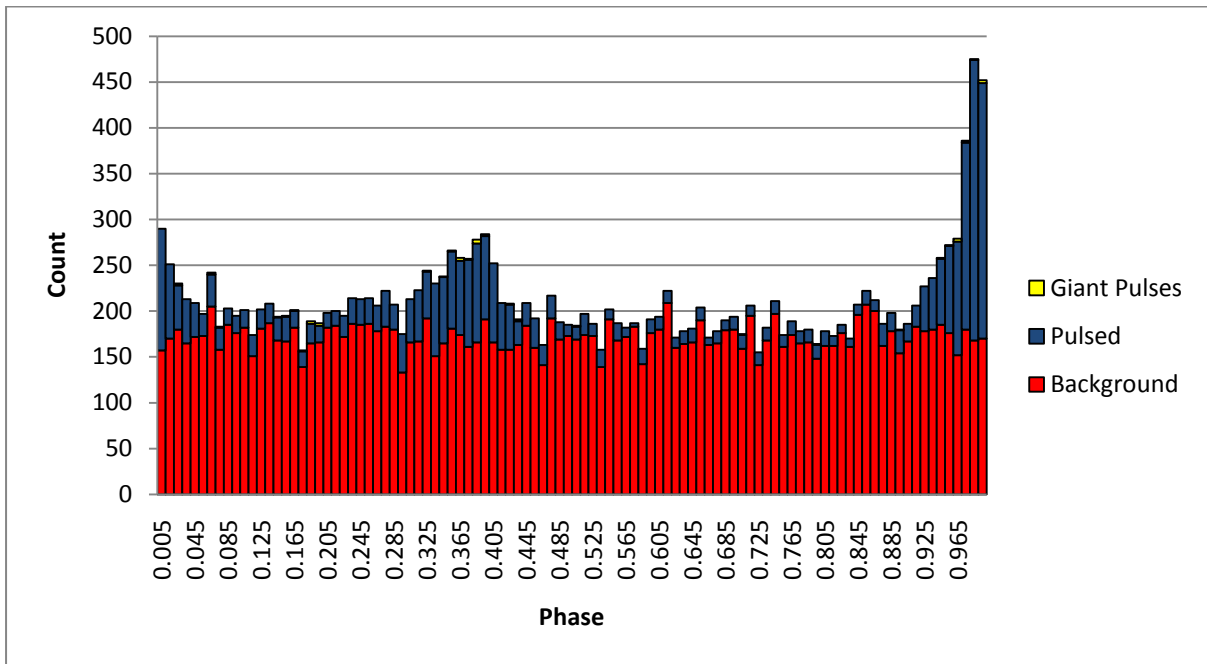
Figure 15: CTA Raue pulse profiles

The pulse profiles for the CTA Raue estimate are shown below. (i): Fermi spectrum with 50 hours of observation time. (ii) MAGIC spectrum with 5 hours of observation times. (iii) Fermi normalisation/MAGIC cut-off energy with 0.5 hours of observation time. (iv) Fermi normalisation/MAGIC decay with 0.5 hours of observation time.

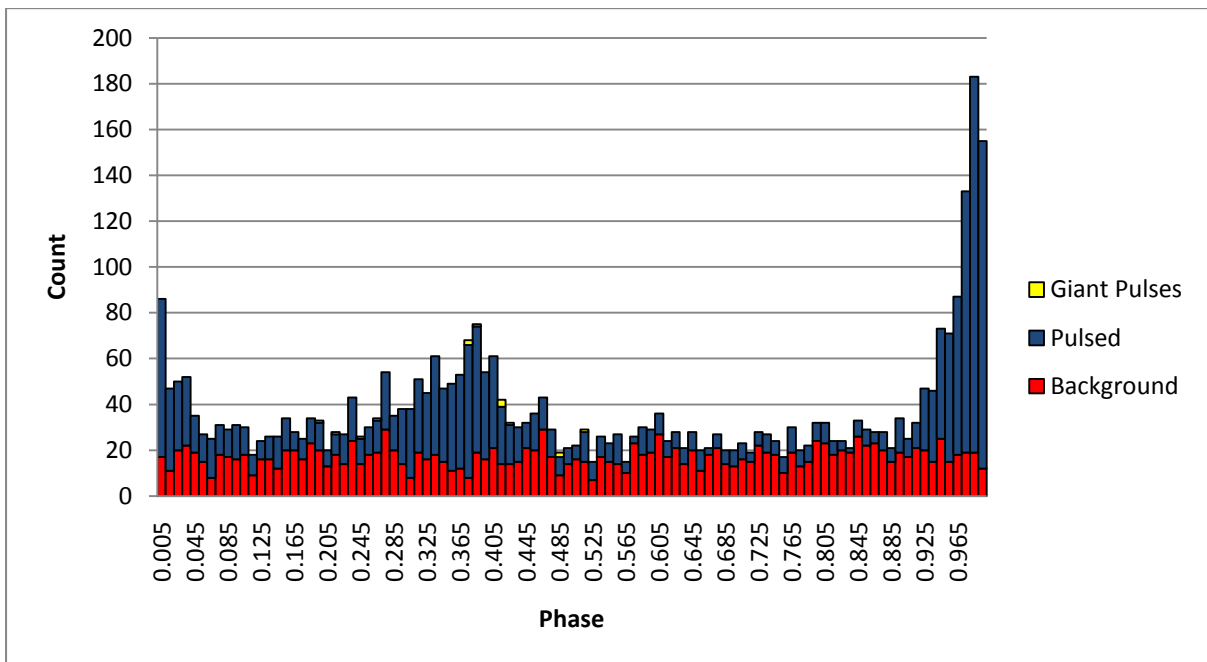
(i)



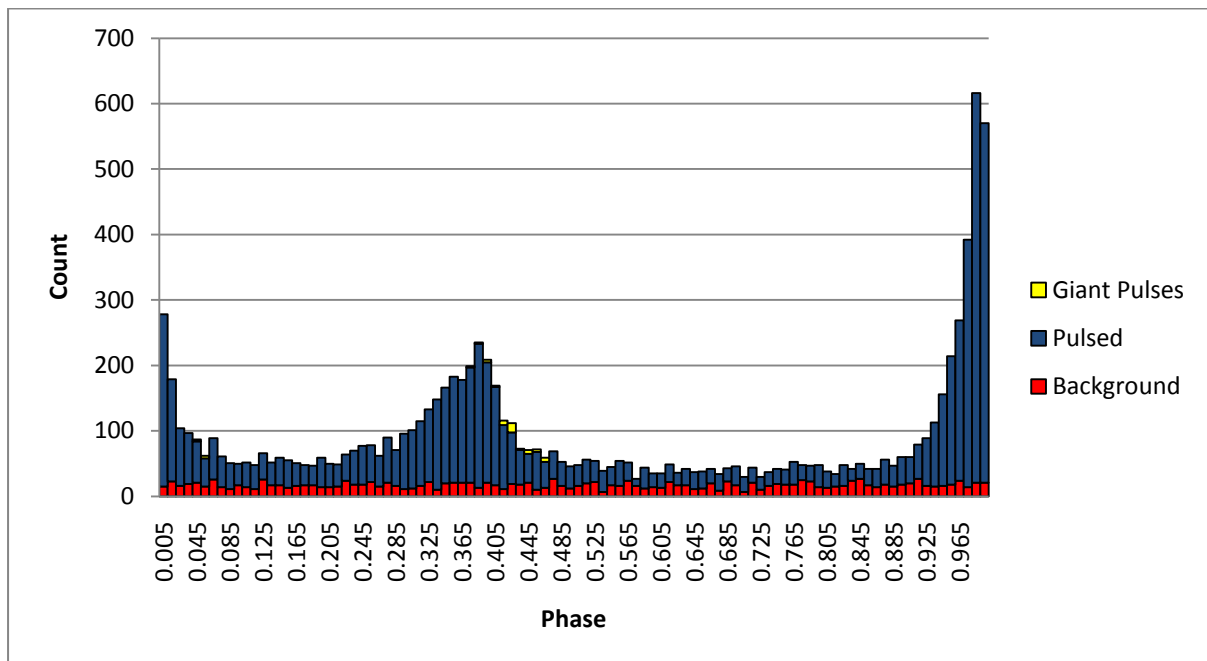
(ii)



(iii)



(iv)



The results for the CTA Raue estimate are typical of all the array estimates, except for 5@5. As the detection rate for the array increases, the time taken to build a good pulse profile drops rapidly, meaning not only that the background count can be reduced, but improving the ability of the array to monitor developments in the pulsar period. For 5@5, there is one major exception to the trend shown in the CTA Raue results, in that the MAGIC spectrum gives poorer results than the Fermi spectrum as a result of the lower detection rate. Outside of this minor aberration, the pattern shown in Figure 17 remains very similar.

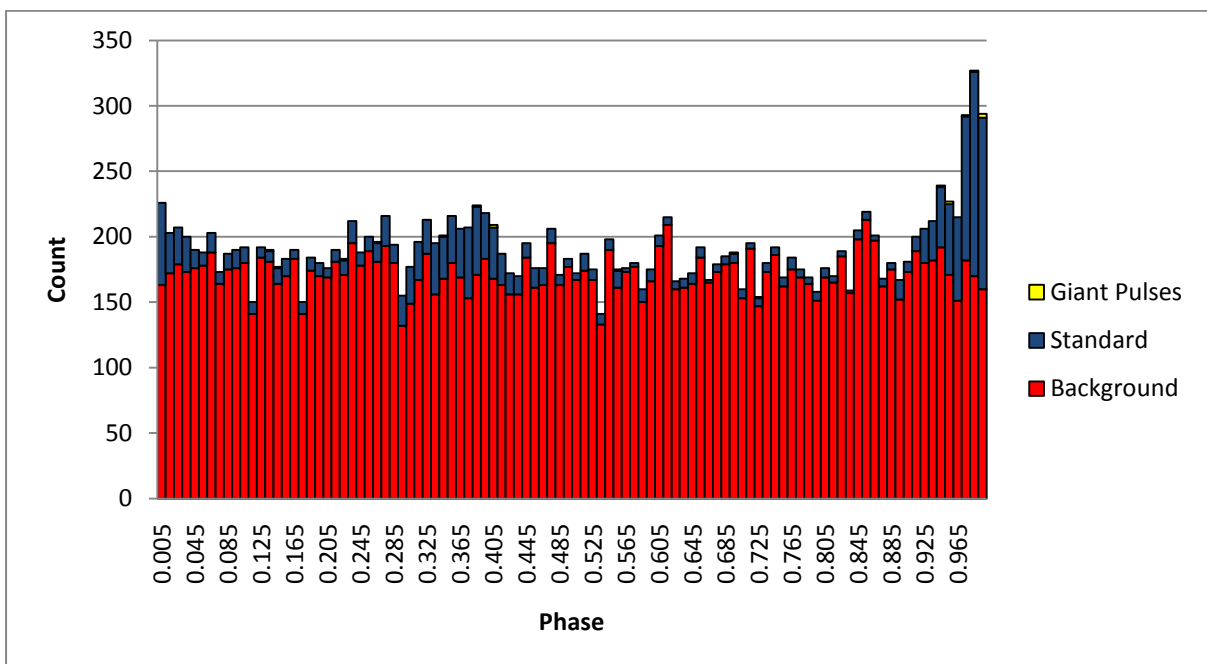
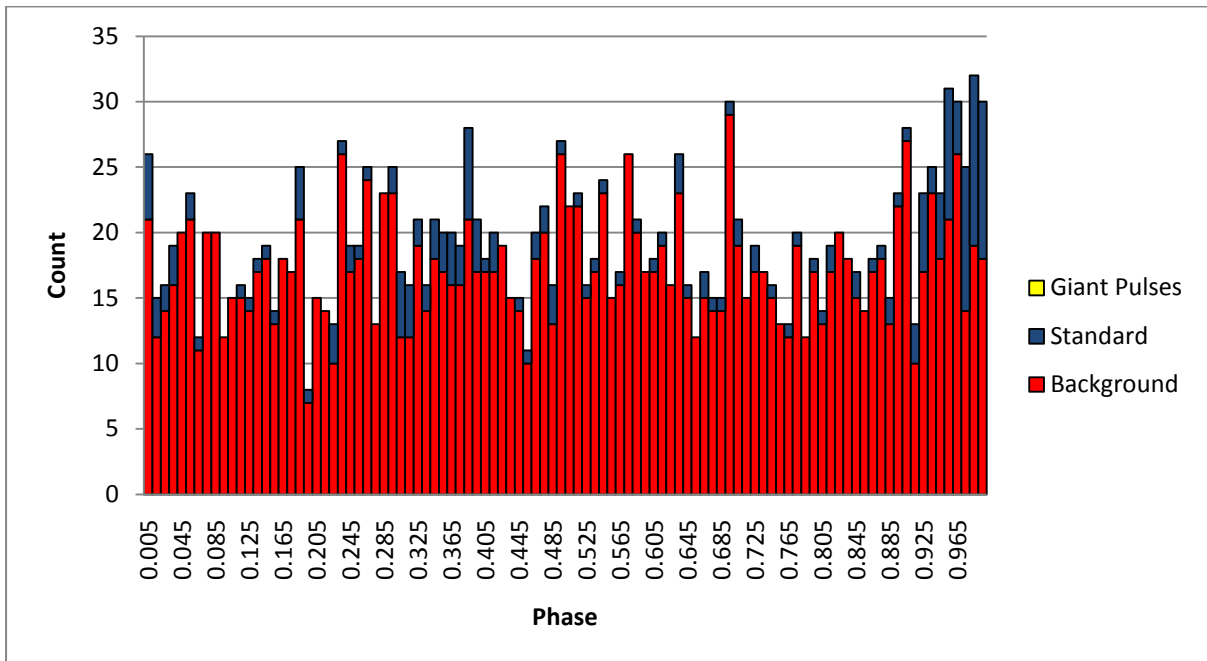
To demonstrate how the pulse profile develops with increasing observation time, Figure 16 shows the development of the light curves for the Fermi spectrum using the CTA Raue estimate. The evolution of features from the noise is apparent. The results here are typical for all the array/spectra combinations, if suitable observation times are chosen to give each step. These results are displayed as they are the results that most closely resemble what the CTA should be capable of, and they showcase the evolution of the observed pulse profile very well.

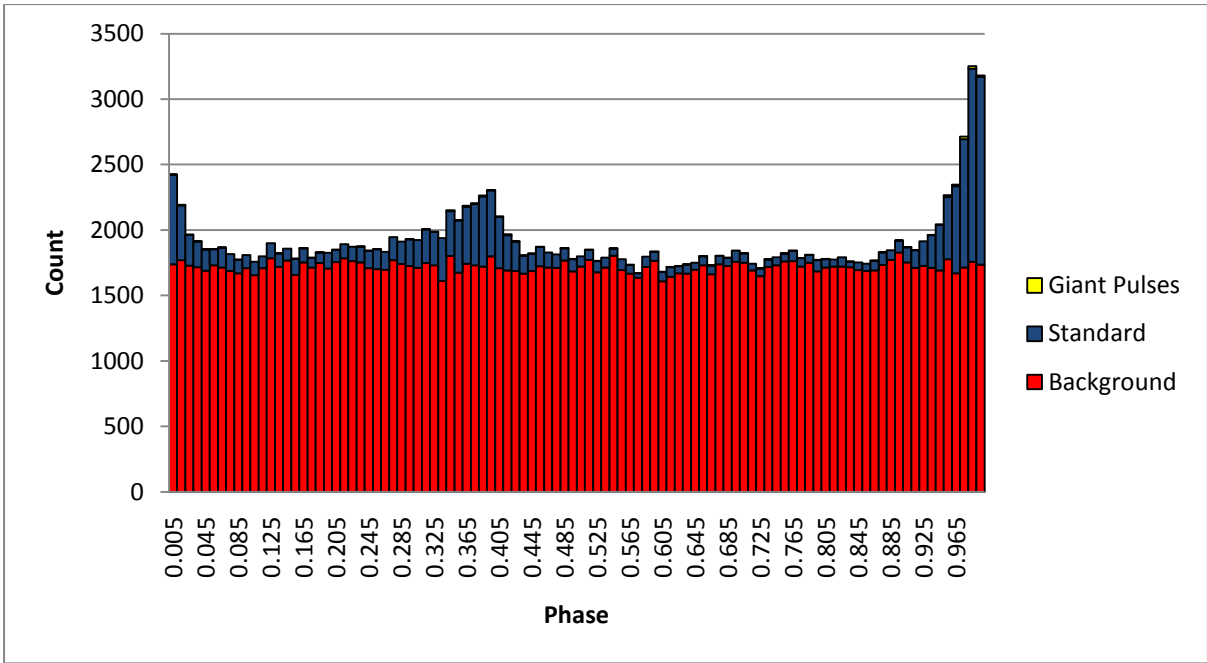
The first plot, showing the results of 0.5 hours of observations, give very little useful data, though with the benefit of the differentiation between pulsed and background photons, it is possible to see the P1 pulse beginning to form. After 5 hours of observations, the P1 peak is clearly visible, and the P2 peak is beginning to appear as a detectable object. The final, 50 hour, plot shows the full pulse profile expected from the Crab, with all features being clearly defined.

The CTA Abramowski estimate represents the best case scenario for the CTA, combining a large effective area with a low energy threshold, and as such produces very good results on very short timescales, as shown in Appendix I Figure 3. The P1 and P2 peaks can be easily resolved with observation times of less than 5 hours, in most cases less than 0.5 hours, again giving the possibility of investigating pulse period development over time. The results depicted here are unlikely to be achieved by the actual CTA array, as this estimate is quite optimistic.

Figure 16: Pulse profile development for the Fermi spectrum with CTA Raue

From top to bottom: 0.5, 5 and 50 hour observation time pulse profiles for the CTA Raue estimate using the Fermi spectrum.





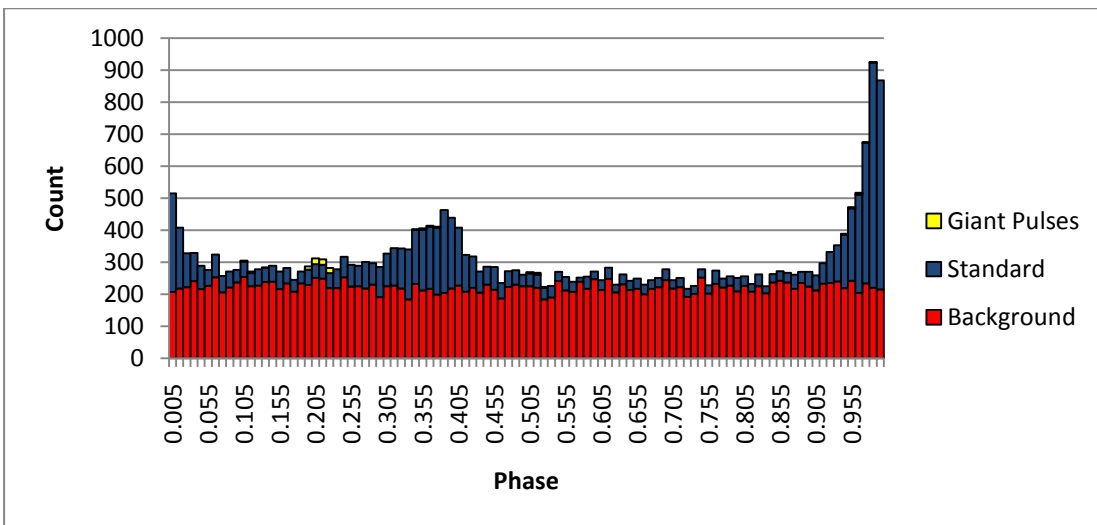
5@5 light curves for all four spectra are given below in Figure 17. The impact of the increased detection can clearly be seen, both in the count and the clarity of the pulse profile gained within a short time frame.

These results clearly demonstrate the power of the 5@5 array to rapidly resolve pulse profiles, and as such show its power as a tool for pulsar observations. One point to note from these, and indeed all of the results, is that the contribution of giant pulse photons to the pulse profile is insignificant in comparison to the background and pulsed contributions.

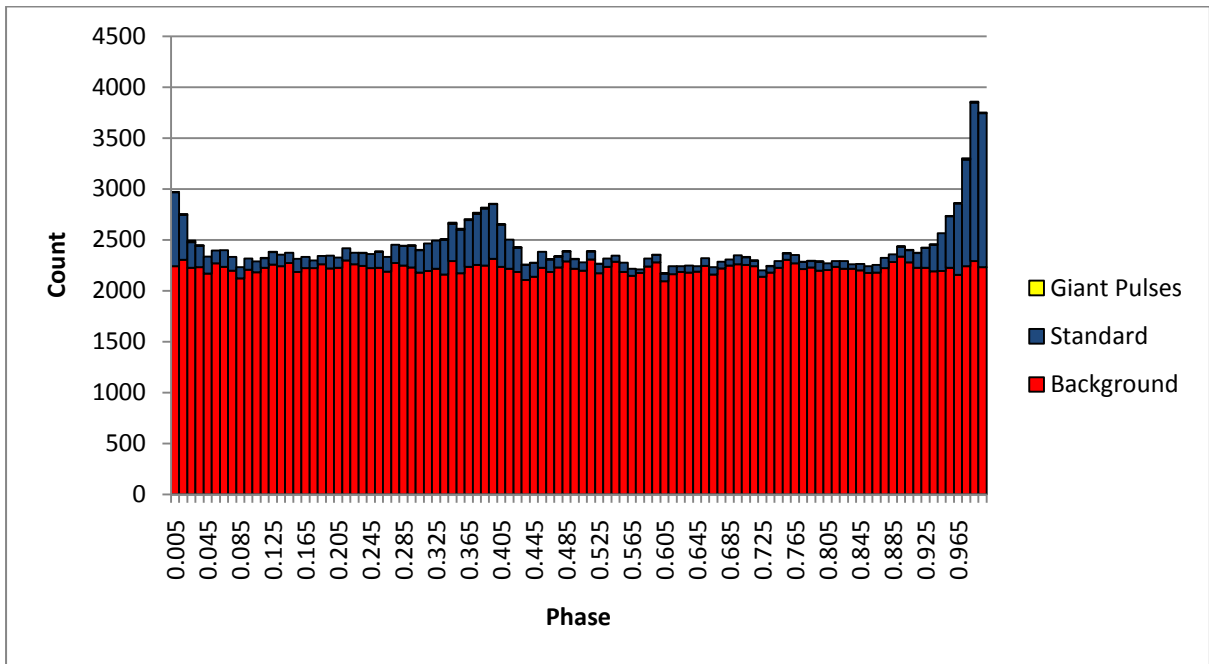
Figure 17: 5@5 pulse profiles

(i): Fermi spectrum with 0.5 hours of observation time. (ii): MAGIC spectrum with 5 hours of observation. (iii): Fermi normalisation/MAGIC cut-off with 0.5 hours of observation (iv): Fermi normalisation/MAGIC decay with 0.5 hours of observation time.

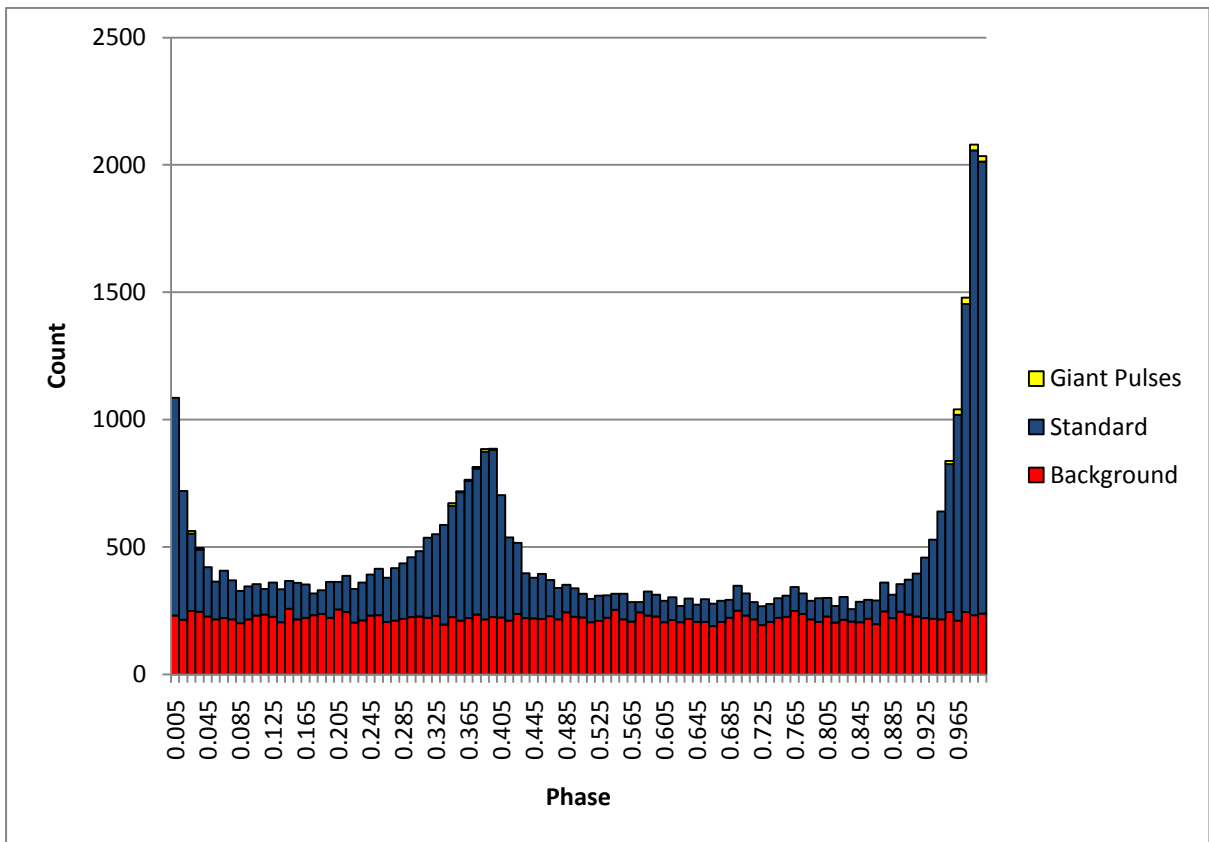
(i)



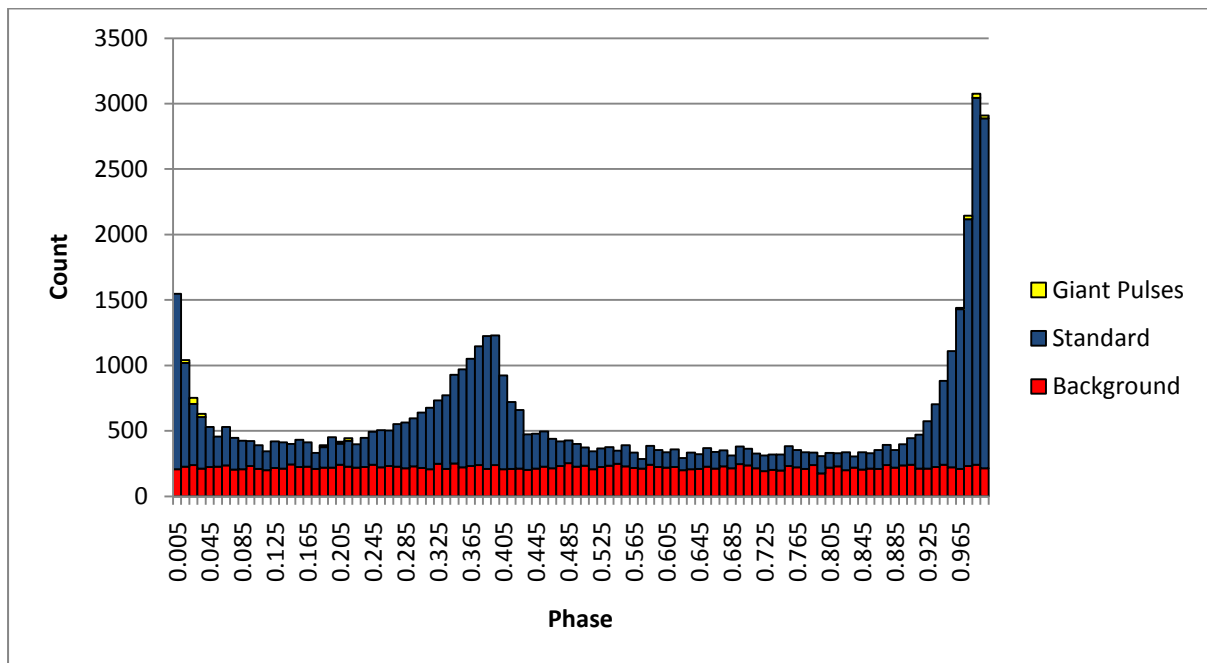
(ii)



(iii)



(iv)



4.2 Direct Observations of Giant Pulses

The number of expected coincidences and giant pulses for each array was calculated for three levels of detection requirement, namely 3, 4 and 5 photons per 4 phase bin block for a 50 hour observation period for each of the three sections of the pulse profile. For each array, the most promising threshold results are tabulated below, with “most promising” being defined as the results that give the highest proportion of giant pulses to coincidences, whilst retaining, if possible, some possibility of actually being able to observe the giant pulses in a reasonable observation time.

For CTA LET the most promising results were hard to determine, as many of the spectra gave no chance of detecting a giant pulse by direct observation, the magnitude of the giant pulses required being just too high. The calculations with $n=4$ gave two results that would be potentially detectable, with sufficient observation, in the inter-pulse region so these were selected as the most promising candidate signal. 5 photon signals were also present, although these occurred at an even lower rate than the $n=4$ signals, so were disregarded. In the P1 and P2 regions, the rate of coincidence events was much higher proportionally, so any signal would be swamped with noise, even though the expected number of giant pulses was higher than in the inter-pulse region.

Table 5: Expected number of direct observations for CTA LET

| Number of 4 photon signals in a 4 phase block for CTA LET over a 50 hour Observation Period in the Inter-pulse region | | |
|---|-------------------------------------|-------------------------------------|
| Spectrum | Giant Pulse Count | Coincidence Count |
| Fermi | 0_{-0}^{+0} | 0_{-0}^{+0} |
| MAGIC | 0_{-0}^{+0} | 0_{-0}^{+0} |
| Fermi spectrum with MAGIC cut-off energy | $6.1_{-6.1}^{+60.1} \times 10^{-4}$ | 0_{-0}^{+0} |
| Fermi spectrum with MAGIC super-exponential cut-off | $2.4_{-2.0}^{+4.8} \times 10^{-2}$ | $2.0_{-2.0}^{+18.0} \times 10^{-5}$ |

For CTA Abramowski and CTA Raue, the n=5 calculations gave some promising results, especially in the inter-pulse region. Again, although the expected numbers of giant pulse detections was greater in P1 and P2, the boost in the rate of pulsed photon detections outweighed the increase in proportion of giant pulses occurring in these regions greatly.

Table 6: Expected number of direct observations for CTA Abramowski

| Number of 5 photon signals in a 4 phase block for CTA Abramowski over a 50 hour Observation Period in the Inter-pulse region | | |
|--|-------------------------------------|-------------------------------------|
| Spectrum | Giant Pulse Count | Coincidence Count |
| Fermi | $5.5_{-5.5}^{+22.1} \times 10^{-3}$ | $5.3_{-0.7}^{+2.0} \times 10^{-4}$ |
| MAGIC | $9.1_{-5.8}^{+7.7} \times 10^{-2}$ | $1.3_{-0.1}^{+0.1} \times 10^{-3}$ |
| Fermi spectrum with MAGIC cut-off energy | $7.0_{-5.7}^{+15.7} \times 10^{-1}$ | $1.0_{-1.0}^{+18.0} \times 10^{-1}$ |
| Fermi spectrum with MAGIC super-exponential cut-off | $5.8_{-4.3}^{+9.5}$ | $2.5_{-2.4}^{+46.1}$ |

Table 7: Expected number of direct observations for CTA Raue

| Number of 5 photon signals in a 4 phase block for CTA Raue over a 50 hour Observation Period in the Inter-pulse region | | |
|--|------------------------------------|-------------------------------------|
| Spectrum | Giant Pulse Count | Coincidence Count |
| Fermi | $2.0^{+6.6}_{-2.0} \times 10^{-3}$ | $7.4^{+4.1}_{-1.7} \times 10^{-7}$ |
| MAGIC | $8.3^{+7.4}_{-5.7} \times 10^{-3}$ | $1.1^{+0.5}_{-0.4} \times 10^{-6}$ |
| Fermi spectrum with MAGIC cut-off energy | $1.0^{+1.8}_{-0.8} \times 10^{-1}$ | $1.6^{+11.9}_{-1.3} \times 10^{-5}$ |
| Fermi spectrum with MAGIC super-exponential cut-off | $6.1^{+9.1}_{-4.3} \times 10^{-1}$ | $1.1^{+14.5}_{-1.0} \times 10^{-3}$ |

For 5@5, again the n=5 inter-pulse results are the most promising, although they are extremely poor, but it is possible, given 5@5's higher detection rates, that a higher threshold for identification could result in better results, although time constraints have not allowed this evaluation to be performed.

Table 8: Expected number of direct observations for 5@5

| Number of 5 photon signals in a 4 phase block for 5@5 over a 50 hour Observation Period in the Inter-pulse region | | |
|---|------------------------------------|------------------------------------|
| Spectrum | Giant Pulse Count | Coincidence Count |
| Fermi | $7.8^{+6.1}_{-4.0} \times 10^{-1}$ | $4.1^{+3.9}_{-1.8} \times 10^{-1}$ |
| MAGIC | $9.8^{+2.1}_{-2.5} \times 10^{-2}$ | $1.2^{+0.1}_{-0.1} \times 10^{-1}$ |
| Fermi spectrum with MAGIC cut-off energy | $3.1^{+2.0}_{-1.5}$ | $2.83^{+4.8}_{-0.2}$ |
| Fermi spectrum with MAGIC super-exponential cut-off | $5.6^{+3.2}_{-2.4}$ | $9.4^{+17.4}_{-6.3}$ |

4.3 Statistical Interval Analysis

For each array/spectrum combination, Statistical Interval Analysis was performed with a time chosen to suit the detection rate of the array. To avoid inordinately long computing times whilst retaining meaningful results for all arrays, higher detection rate arrays were simulated for shorter observation periods than arrays with poorer performance. The plots shown below show two bars for each phase bin, the bar in red shows the results of the background and pulsed photons only, in other words the result if that giant pulses are not present. The blue bar shows what the simulation shows would be seen when giant pulses are present. Again, in reality, we would not be able to make this distinction directly, but the trends we see in each of the curves should be replicated, allowing us to infer the presence of giant pulses.

For the CTA LET estimate, neither the Fermi nor the MAGIC spectrum showed any clear results, as shown in Appendix II Figure 1 for the Fermi spectrum, presumably because even the largest giant pulses did not result in the detection of more than one photon. Using the hybrid spectra, results could be obtained, as shown in Appendix II Figure 2 for the Fermi normalisation with the MAGIC decay.

Using the CTA Raue estimate, which roughly simulates the pre-cut CTA or the CTA with high efficiency low energy cuts, the prospects for SIA are much better. Figure 18 below shows the results for all four spectra, each of which shows a clear signal. Even after 0.5 hours, the giant pulse photons have produced a peak of 24 results, which is an excess of 14 counts over the value due to non-giant pulse photons, and around ten counts above the approximate mean value of counts per interval bin.

These results demonstrate the strengthening of the signal as the detection rate increases, with the lowest detection rate in the top plot and the highest in the bottom. The suppression in background noise as the rate increases is also clear. The CTA Abramowski estimate also gave good results, as again the detection rate increases, in around 5 to 10 hours, depending on the spectrum examined. Appendix II Figure 3 shows the plot of the SIA results for 10 hours of observations of the MAGIC spectrum, and Appendix II Figure 4 shows the results of SIA on five hours of observations of the Fermi normalised MAGIC decay spectrum.

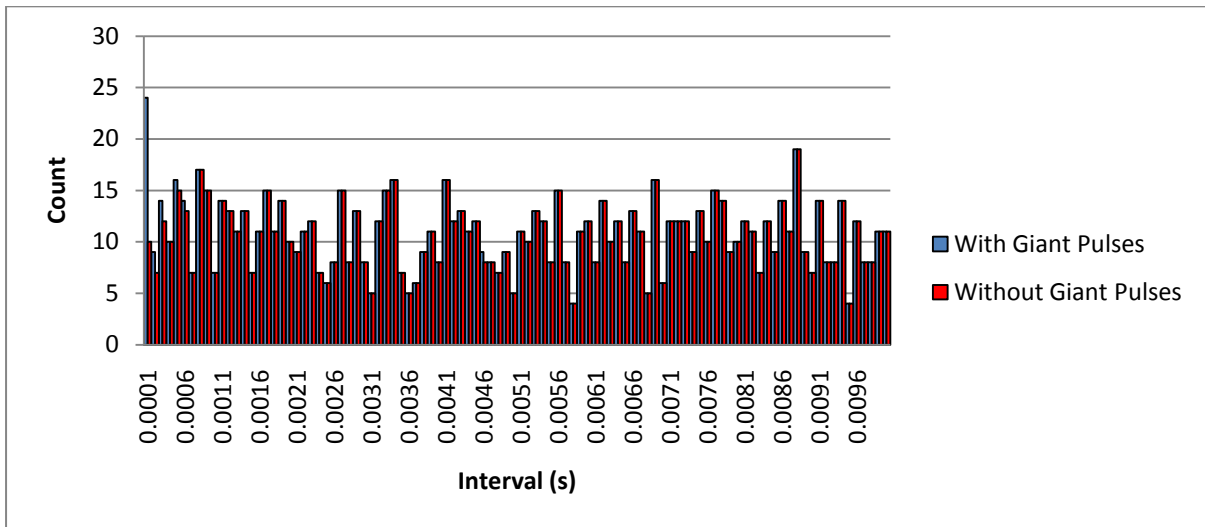
For 5@5, the higher rate of data collection allows for clear data to be gathered in a very short time. Figure 19 shows the results for 0.5 hours of emission with all four spectra. In all the signature of the giant pulses is clearly visible. Even in the worst case, with the MAGIC spectrum, there is an excess of around 60 events above the expected count in the lowest interval bin. For the hybrid spectra, the peaks are far greater, of the order of 500 counts over the expected level.

In these results the exponential fall off in intervals expected from the background and pulsed photon contribution is also visible, as the average interval is much shorter than for the other arrays, resulting in a more rapid decay.

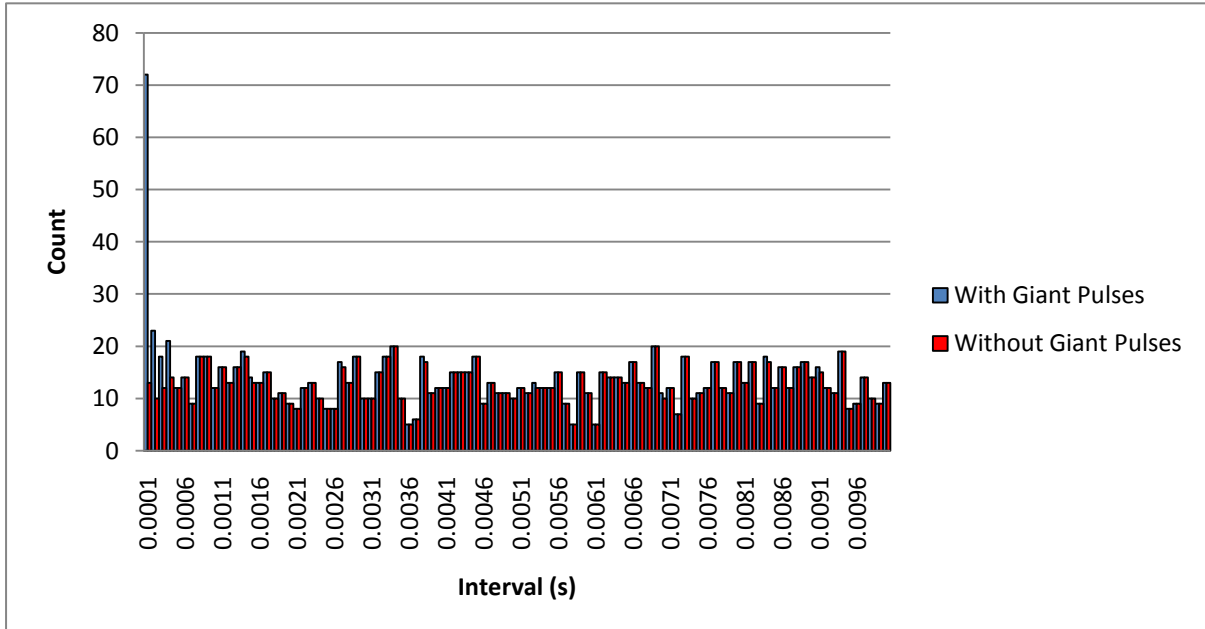
Figure 18: SIA results for CTA Raue

The results of performing SIA on simulated observations with the CTA Raue estimate of the (i) Fermi spectrum for 25 hours (ii) MAGIC spectrum for 25 hours (iii) Fermi normalisation/MAGIC cut-off spectrum for five hours (iv) Fermi normalised MAGIC decay spectrum for five hours. In all four, the signal of the giant pulses can clearly be seen as a deviation from the expected pattern of intervals. In the case of (i), the results are fairly noisy, which could be improved by longer observations, but even in this case the signal is significantly larger than the noise. In (iv) the decay is most clear, actually showing something of a curve rather than the more or less even distributions in (ii) and (iii).

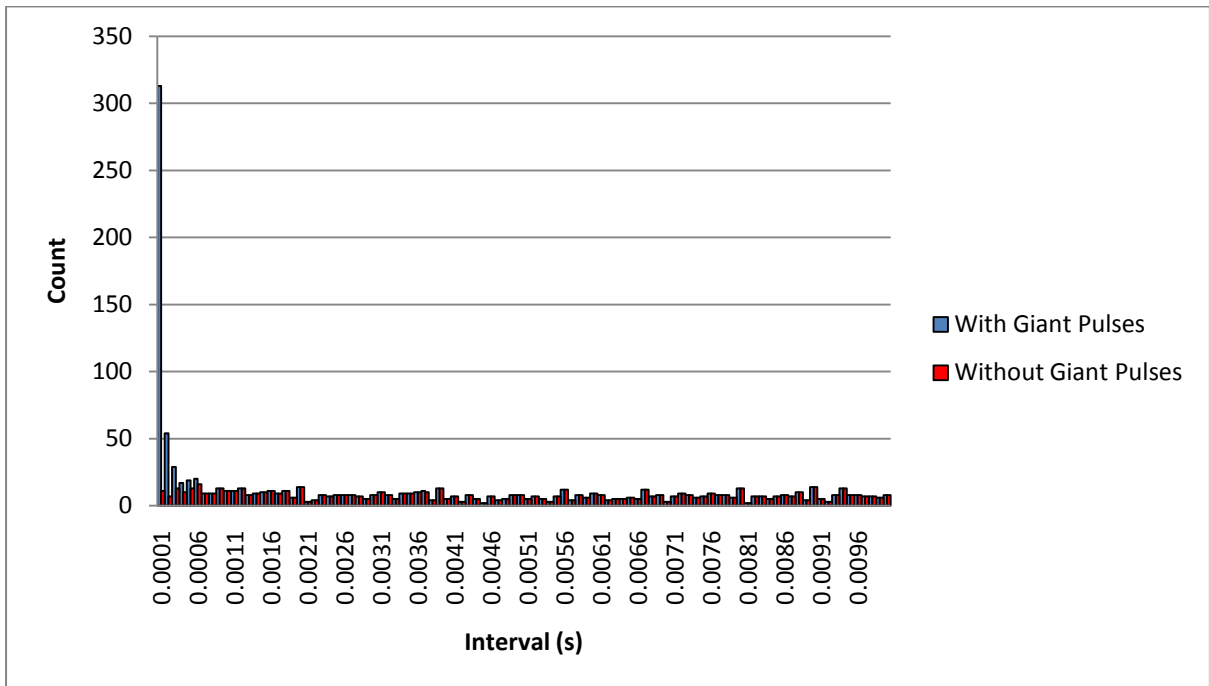
(i)



(ii)



(iii)



(iv)

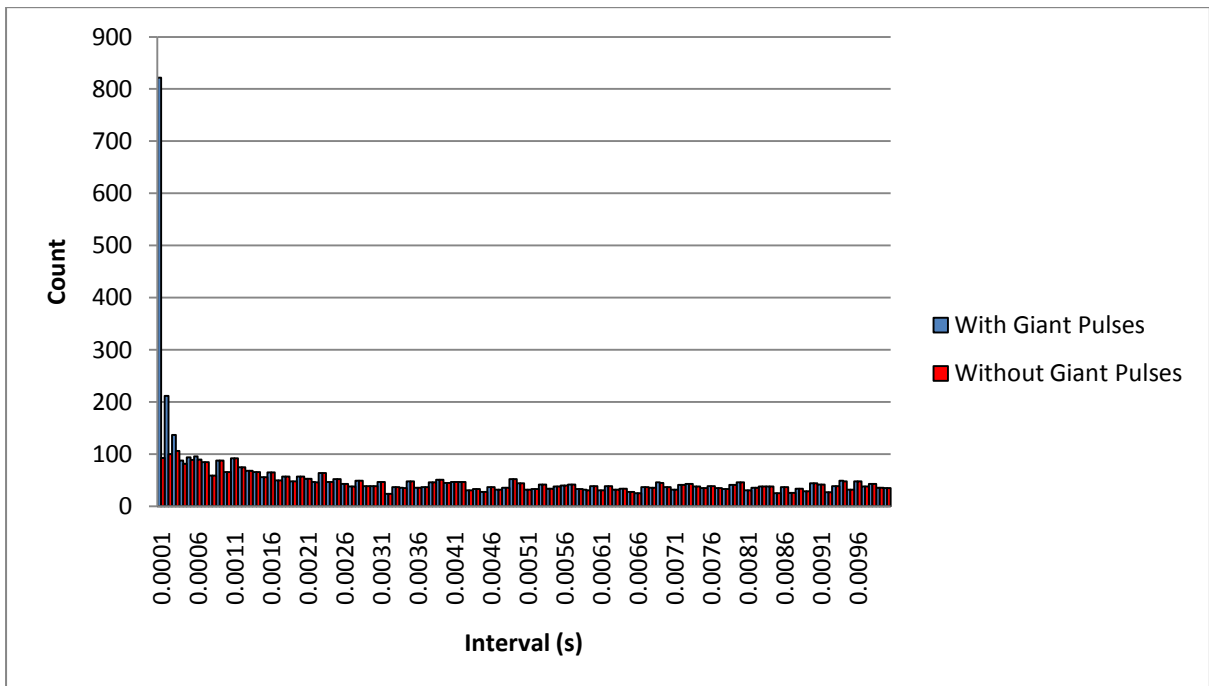
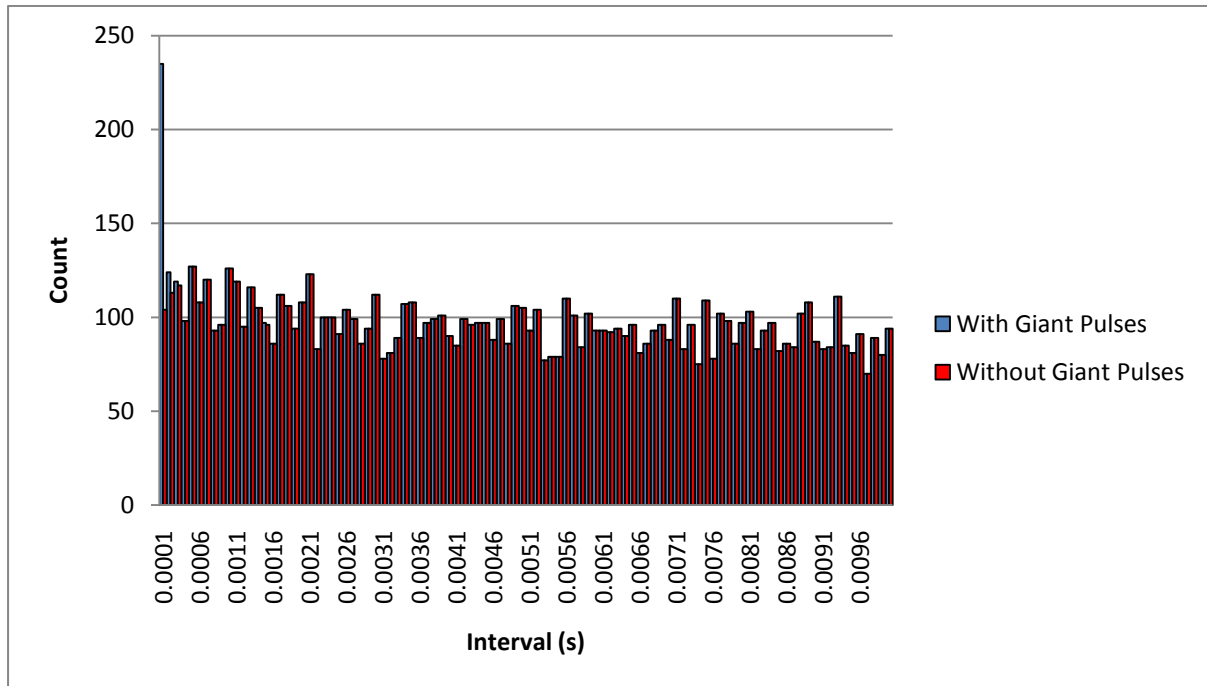


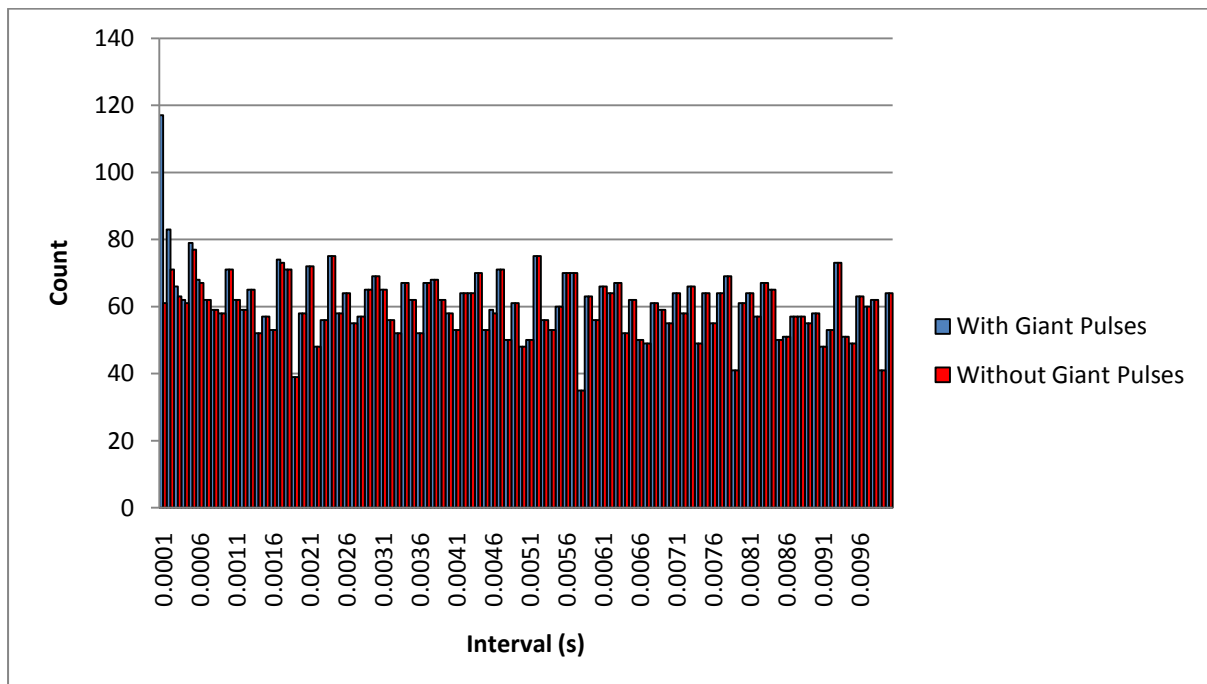
Figure 19: SIA results for 5@5

The results of SIA on 0.5 hours of 5@5 observations of the (i) Fermi (ii) MAGIC (iii) Fermi normalisation with MAGIC cut-off and (iv) Fermi normalised MAGIC decay spectra are shown here. In all the peak associated with the presence of giant pulses can be clearly seen, and the decay pattern expected from the intervals is also clearly visible in (iii) and (iv), as the higher detection rate results in a shorter characteristic time for the decay.

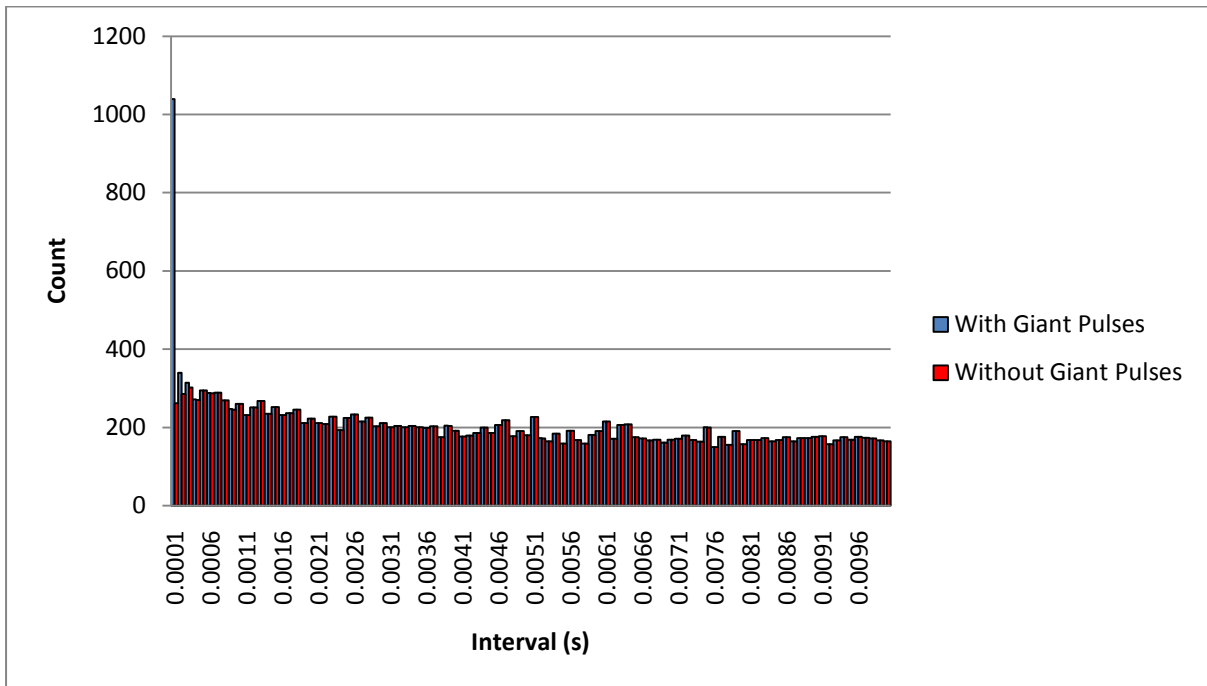
(i)



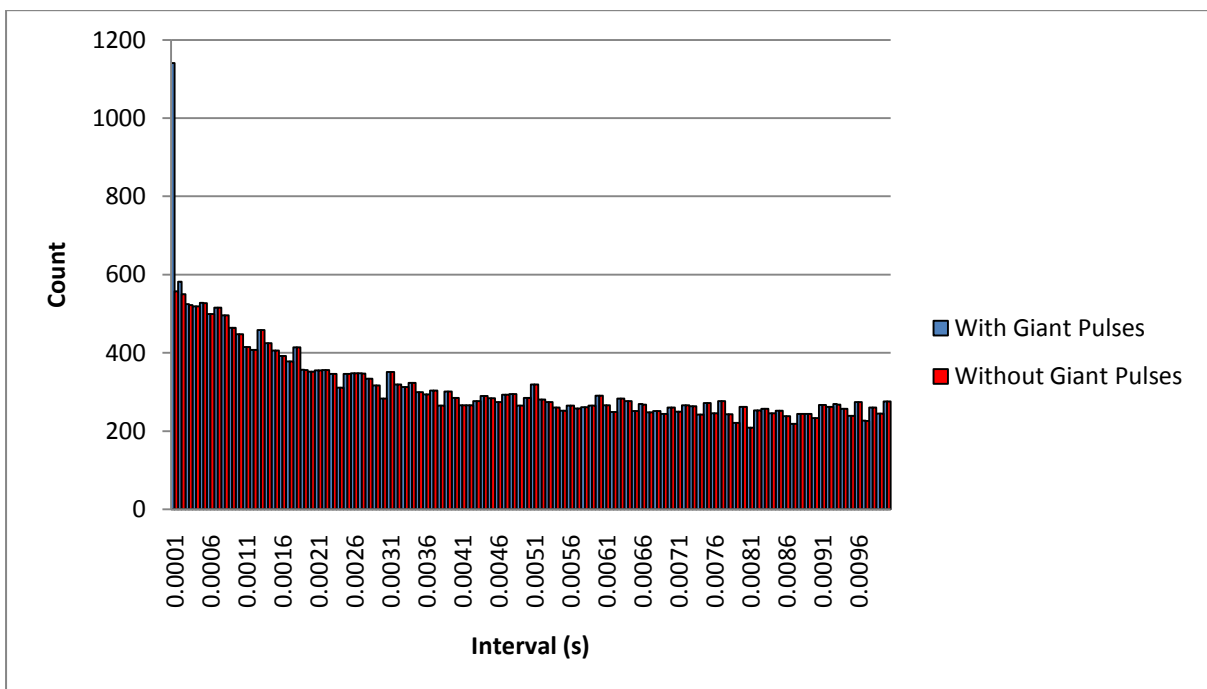
(ii)



(iii)



(iv)



4.4 Signatures of Emission Modes

The simulation of pulse profiles assuming short duration giant pulses produced near identical results to those of the simulations using the standard length giant pulses, with some small differences to

the distribution of the giant pulse photons, which, as can be seen in the light curves in Section 4.1, are of only limited significance to the pulse profile.

To model a scenario where gamma-photons are only produced in giant pulses, an investigation was performed to find what parameters of giant pulses would be able to produce the Fermi spectrum. In the Fermi paper it is indicated that the background rate is around half the detection rate of the instrument (16), so this ratio was maintained in the investigation. The observation time is not clearly stated in the paper, but is taken to be of the order of 10^7 seconds, around half of the total time of the all sky survey. By setting the effective area of the LAT to 0.8 m^2 for all energies, a rather large simplification, a detection rate of $4 \times 10^{-4} \text{ Hz}$ was calculated for the LAT. Halving this gives a background rate of 0.2 mHz . Taking these values, a search for suitable parameters for the giant pulses was begun.

The first parameter examined was the frequency at which giant pulses occur. The frequencies of giant pulses published in the paper by R. Karuppusamy, B.W. Stappers and W. van Straten (25) were taken as a baseline for investigation. In the P1 region, the frequency is reported to have been of order 1.1 Hz (25), and in the P2 region of order 0.2 Hz (25). To give the best chance of being able to replicate the pulse profile by giving the greatest number of giant pulses, the P1 frequency was taken as the standard level. This will cause the rate of giant pulses to be overestimated, so the magnitude range calculated below should be viewed as a lower limit required to reproduce the Fermi results.

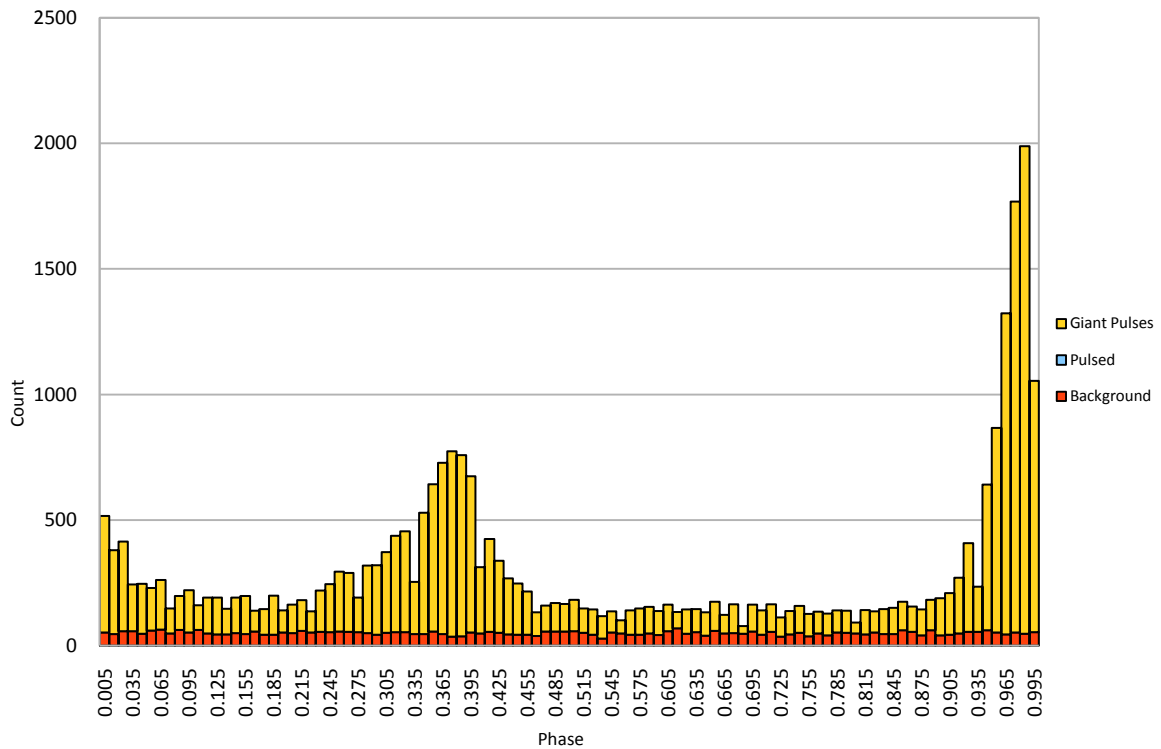
After the frequency was set, a series of simulations was performed, altering the boost to the magnitude distribution of the giant pulses, and the resultant pulse profiles were compared to the Fermi data. The maximum count of the P1 and P2 peaks, and the approximate average count in the inter-pulse phase bins were compared until all three could be matched. As the frequency chosen is high, it was expected that the inter-pulse phase bin counts and the P2 count would be somewhat higher than the real values from the Fermi pulse profile when the P1 count matched, so a slight overshoot in these two values should not be looked upon as a contradiction to the emission model, more as a failing of the simulation performed here.

Due to time constraints, a more thorough search for other possible combinations that would also replicate the results was not made. The results determined from these parameters are therefore only one of the possible results that could be obtained, and should be treated with a degree of caution.

Figure 20 below shows the final result of this investigation, where the giant pulse magnitude distribution is boosted to one hundred times its normal value, giving a range from 200 up to 5000 times the value of a "standard" pulse. If this emission mode is actually the case, there are no such things as a standard pulse, so the boost must be measured in comparison to the pulses we expect based on the normal emission model.

Figure 20: The pulse profile reconstructed only from background and giant pulse photons

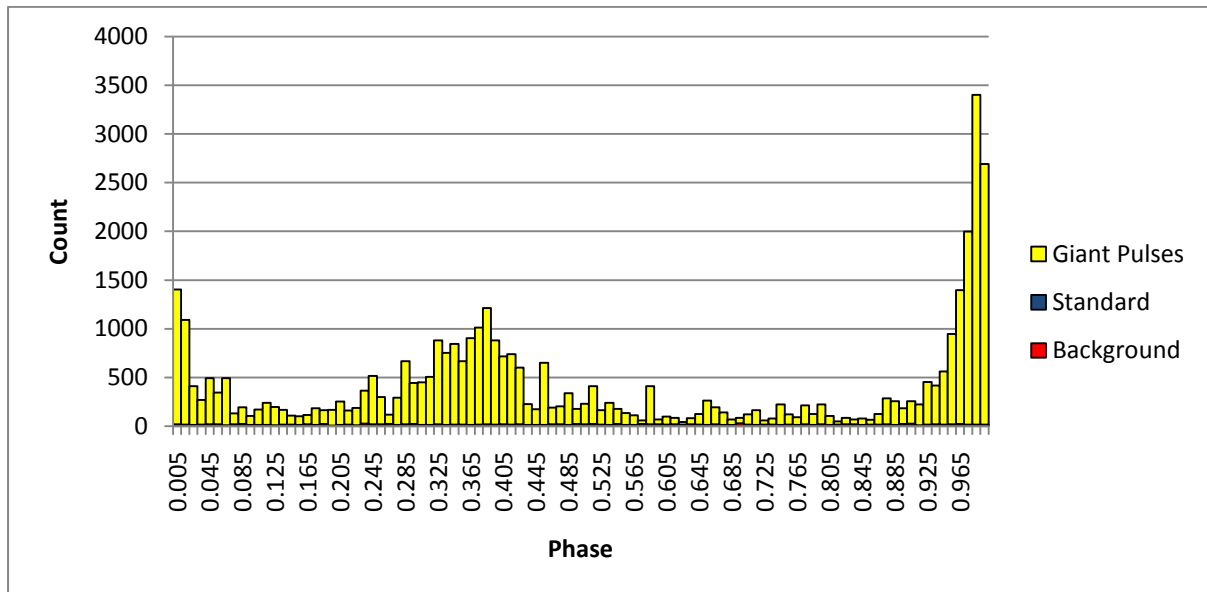
The pulse profile shown below was produced from giant pulse and background photons alone. The values of the P1 peak, P2 peak and the average inter-pulse phase bin counts all conform to the Fermi values. As can be seen, the shape of the pulse profile is also conserved in this emission mode.



With these parameters fixed as the new giant pulse model, simulations of observations with the CTA and 5@5 were run for 0.5, 5 and 50 hour observation times. The results were compared and some interesting differences were identified. In Figure 21 below, the results of 0.5 hour observations for the CTA LET and CTA Raue estimates are shown. It is clear that the pulse profile is far more developed than in the 0.5 hour observations with the standard emission mode, and has a much higher count per phase bin.

Figure 21: CTA Raue pulse profile for the giant pulse only emission mode

The pulse profiles for 0.5 hours of observations using the Fermi spectrum detection rates with the CTA Raue estimates. As can be seen, the profile is significantly more developed than its counterpart from the standard emission mode. The overall count of photons is also increased, contributing to the improved statistics.



This trend is also present in 5@5, amplified further by the higher count rate, as shown in Figure 22. As the average number of photons expected per giant pulse has increased, the pulse profile is a little noisier, as small numbers of large giant pulses can cause significant variation in the count.

The SIA analysis of the new emission mode shows a clearly identifiable signature. The increase in number of giant pulses through the period and the increased strength of the giant pulses creates a significant increase in the count of low intervals. Additionally, the loss of the pulsed photons leads to a decrease in the number of intervals due to photons not associated with giant pulses, which will decrease the background distribution. Figure 23 below shows SIA results for the CTA Raue with the Fermi spectrum, which clearly shows the boosted signal completely overwhelms the background and pulsed photons.

Figure 22: 5@5 pulse profiles for the giant pulse only emission mode

The pulse profile of 0.5 hours of observations with the 5@5 array using the Fermi spectrum detection rates. As can be seen, the pulse profile is very clear and the count has been massively increased.

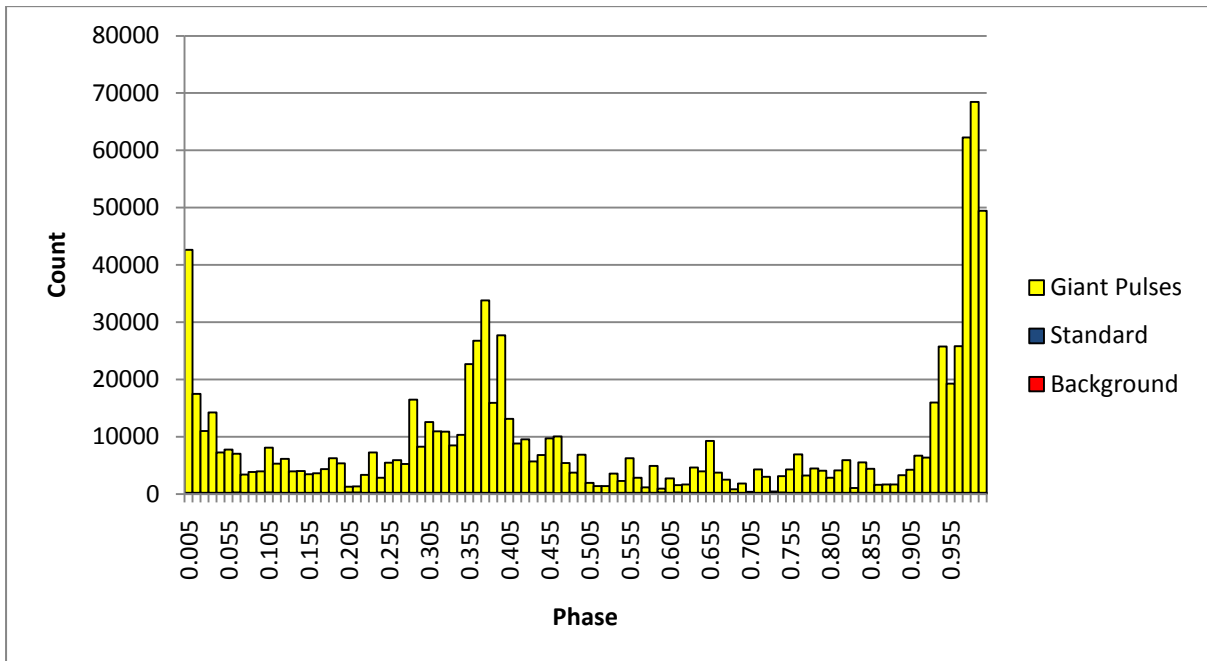
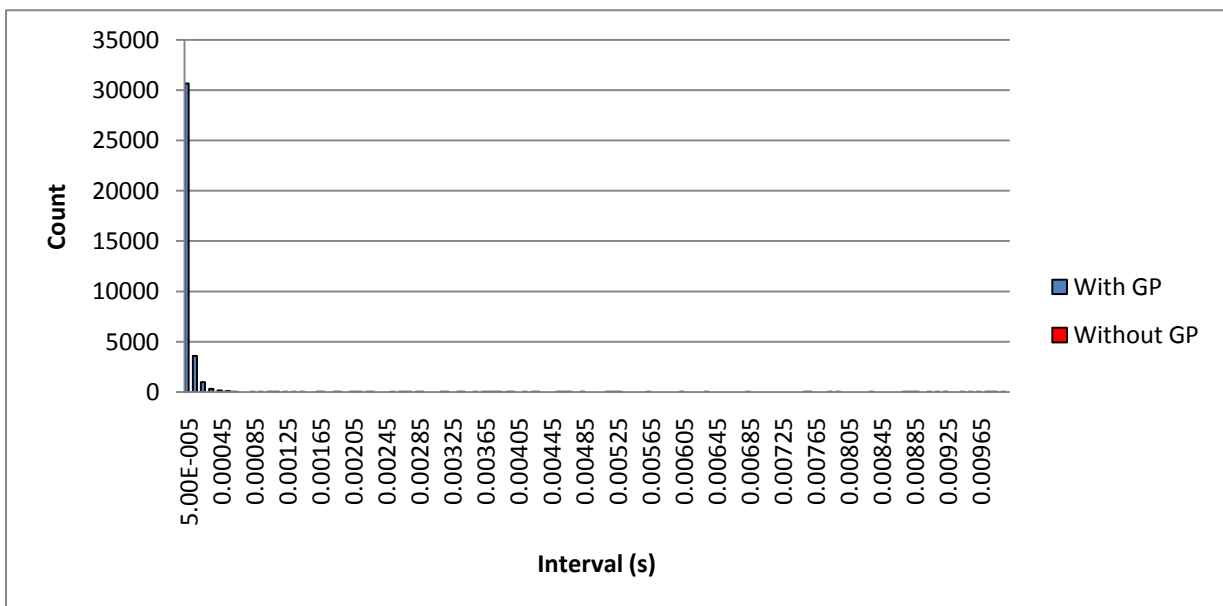


Figure 23: SIA results of CTA Raue observations of the Fermi spectrum with the giant pulse only emission mode

The results of SIA on 10 hours of observations using the Fermi spectrum detection rate with CTA Raue are plotted below, showing the alterations in the SIA caused by the emission mode. The spike associated with the giant pulses is more pronounced and the count of other intervals is reduced massively. These differences should allow the clear identification of this emission mode in comparison to the expected mode.



5.0 Discussion

In this section, the results presented above will be discussed, with regards to their application to the observation of giant pulses, examining the performance for the purposes they are designed for in comparison to current instruments and, where relevant, their general application to pulsar astronomy. The failings and limitations of the methods and results will also be examined, aiming to give a view of the reliability and applicability of the results.

5.1 Simulated Light Curves

From the light curves shown in Section 4.1, it is clear that the clarity of the pulse profile is dictated by the detection rate, with higher detection rates giving a clearer pulse profile in a shorter period. In comparison to Fermi, which has collected around 20 000 photons in eight months of surveying, although not all of this time would have had the Crab in view. The simulations indicate that CTA and 5@5 could collect this many pulsed photons in a matter of hours of observations, in the case of 5@5 or CTA Abramowski and Raue with the hybrid spectra, even in a single nights observations. With this level of timing detail, it could be possible to examine the evolution of the pulsar's period in the gamma range with a fair degree of accuracy, allowing for comparison with the radio behaviour.

The evolution of the pulse profiles over time, as shown in Figure 16, is common to all of the telescopes. At first the profile is dominated by noise, which is then gradually smoothed out as the background count per phase bin approaches a mean value, the with pulsed component becoming increasingly clear above this. In the example here, the P1 peak becomes clear after five hours, but is at least partially visible after 0.5 hours. The P2 peak emerges after five hours, though is not clearly defined after this time, whereas after 50 hours it is very clearly visible. Even where the detection rate of pulsed photons is far smaller than the background rate, the pulsed components can be seen clearly above the background results after a sufficient observation time. The best results are achieved, however, when the detection rate is around or higher than the rate at which background photons are detected. It is also clear that giant pulse photons do not significantly alter the distribution of the pulse profile, as they are infrequent events, and rarely occur at the same phase. From this, we can deduce that giant pulses will be difficult to detect from the pulse profiles themselves.

From the plots, we can see that a conservative estimate of the number of background events per phase bin could be found for any of the plots, which could be used to cut away a large portion of the background count, leaving all of the signal count intact. For Figure 14 (ii), for example, we could make a cut at 100 counts per bin, saying that this is the minimum expected background per bin, and lose none of the signal data. The level at which the cut should be made would be simple to find, by multiplying the background rate by the observation time and dividing by 100, we would have the number of background events per bin. Reducing this value by, say, 25% to allow for variation would give a reasonably conservative expected count per bin, which would remove around 75% of the background events. For a longer time of observation, this method could be used to reduce the background count to 10 or even 5% of its actual value.

In the 5@5 pulse profiles however, where a good pulse profile can be built in a very short time, giant pulses could produce a pronounced and detectable signal. As the background rate is very high, large variations in the background count will be unlikely, as the background is evenly distributed. Meanwhile, giant pulses can easily cause variations on the order of tens of photons, which would show up in most sections of the pulse profile as a significant spike. By examining data from a 5@5 type array in small sections, it could be possible to see these spikes, and directly see giant pulses in the light curve.

Given the rate at which data could be collected using these new arrays, it is clear that even fine features in the pulse profile could be detected. With longer observations, far more detailed pulse profiles, perhaps with phase bins one tenth of the current size could be produced, allowing for a far more detailed examination of the emissions from the pulsar. The increased rate of detection will also be a boon in the observation of other, fainter, pulsars, as this will allow for the building of pulse profiles for a bigger proportion of the known pulsar population. This could allow new insight into the behaviour of pulsars, and open up new testing ground for emission models.

These light curves will probably differ significantly from any actual observations of the Crab for one significant reason: the failure of the model to accurately follow the changing morphology of the pulse profile with increasing energy. The morphology detected by MAGIC will probably dominate over the Fermi type morphology used to build the model as the energy range of the arrays being simulated is much closer to the MAGIC range, and Fermi's statistics for the upper reaches of its energy range are very poor. Although the actual morphology of the plots would alter, however, the improvements in count rate should hold. The arrays will still represent a massive improvement, allowing the building of pulse profiles over far shorter timescales than those currently achievable.

5.2 Direct Observation of Giant Pulses

From the results presented in Section 4.2, it can clearly be seen that direct observations of giant pulses faces some serious challenges. The most pressing of these is the background of coincidental detections, which, at low count thresholds, dominates far above the actual signal. The reason for this high expected background count is the number of phase bin blocks that are present, and the ability of each pulsed and background photon to contribute to potentially as many as 4 blocks. This boosting factor, which, it should be noted, neglects the signals from events where background or pulsed photons and a single giant pulse photon coincide, is so large (of the order of 10^8 in a 50 hour period) that it easily swamps the far less frequent giant pulses.

When a high enough threshold is selected, as in the CTA examples shown here for example, the expected count of giant pulses can be considerably larger than the expected background count. Unfortunately, the rates of the giant pulses are then so low as to make direct observation near impossible. In the cases shown here, the observation times would have to be at least hundreds, if not thousands of hours long to guarantee a detection in all but the most optimistic case.

Ultimately, unless a significant background rejection improvement can be made, or unless giant pulses behave differently in the gamma region than in the radio range, direct observation of giant

pulses with Cherenkov telescopes does not seem feasible, so alternative methods to detect the giant pulses in the data and to observe them directly must be found.

5.3 Statistical Interval Analysis

The data that is presented in Section 4.3 shows clearly that Statistical Interval Analysis can give a very clear indication of the presence of giant pulses, assuming that the giant pulses behave in the manner that is predicted. All of the arrays except for the CTA LET showed evidence for giant pulses with all spectra. Even the CTA LET could produce a signature with all but two of the spectra given enough observation time. The border value for the detection of giant pulses with SIA appears to be around 0.1 Hz, as the two array/spectrum combinations that give detection rates of the order 10 mHz are the two combinations that do not produce viable results. Above this threshold value, SIA is a very useful tool in the search for giant pulses. In the cases of CTA Raue and 5@5, the signals generated are all of very high significance, and should be clearly identifiable in the data produced by the arrays.

The plots show, in the cases of the high rate of detection, the decaying pattern in the interval analysis is apparent, as predicted. The higher detection rates produce a more rapid decay, which allows the pattern to be visible on a shorter timescale. For the lower detection rates, the expected flat or near linear distribution of the intervals is also apparent, where the observation time was long enough to even out the random variation in the system.

The data were also examined for another expected feature, a quasi-periodic signal caused by clustering of the photons in the P1 or P2 peaks. Given the greater likelihood of signals occurring in these regions, intervals of integer pulse lengths, or equal to the time difference between the peaks plus an integer number of full periods would be more likely to occur than other intervals. The time interval between the two peaks is of order 20 milliseconds between the P2 and P1 peaks, and 13 milliseconds between the P1 and P2 peaks. Using coarser interval bins than those used in the SIA results presented, a search for these signatures was made, by extending the intervals examined to higher levels. There was no apparent signature of these periodic features, so the features must be very weak, and being swamped by the variation in the results, or not present at all.

In the search for giant pulses, it is clear the higher the detection rate, the clearer the signal of giant pulses. This is due to two factors; firstly the increased rate of detection causes the distribution of the regular detections to become more defined more rapidly, reducing the noise in the system. Secondly, the giant pulses themselves produce more photons per event. To produce a signal, a giant pulse must produce at least two photons, in order to produce a short interval. When the rate of detection increases, the magnitude of giant pulse required to produce two photons decreases significantly, and as the distribution of magnitudes is a power law, the rate at which the giant pulses that produce signals occur increases massively. Also, the average number of photons produced per giant pulse increases, and as the number of short intervals that are caused by a giant pulse is equal to the number of photons that are detected from the pulse minus one, the number of short intervals that occur increases, further boosting the signal.

The results presented here clearly demonstrate the efficacy of SIA as a tool for searching for giant pulses in pulsars, assuming that the detection rate of the array is high enough to allow the detection of two photons from a single giant pulse at a reasonable rate. The minimum rate required for this to occur appears to be of order 0.1 Hz. Higher detection rates allow for the signatures to be magnified in size significantly, and to be detected after a shorter observation period. Assuming the CTA improves its low energy cuts, the detection of giant pulses should be fairly simple using this method, and 5@5 would be ideally suited to detecting these phenomena, perhaps even in fainter and more distant pulsars than the Crab.

There are some slight issues with this analysis which would need to be addressed for a final answer. Firstly, the form of the giant pulses simulated is very crude and unrealistic. This could be addressed by refining the model to more realistically model giant pulses. Additionally, the relationship between pulse duration and energy would tend to produce a stronger signal, as the shorter pulses tend to be more intense, so would produce more photons. This would compress the photons into a very small time period, creating even smaller intervals than in the model currently. Conversely, longer, less intense giant pulses, which are more common, would produce slightly longer short intervals, which could alter the appearance of the signal to a more extended spike, or maybe a double spike. The effects of this refinement on the substructure of this signal could lead to a method for analysing the relationship of duration to magnitude, which could in turn lead to a method of identifying the typical duration of gamma-ray giant pulses.

5.4 Emission Mode Signatures

From the available simulations, the duration of the giant pulses should not cause a significant difference in the pulse profile detected by the arrays. Where the duration of the giant pulse may be significant is for SIA and direct observation of giant pulses. In the SIA, it would produce a potentially much clearer peak, as the photons will be, on average, more tightly contained. For direct observations, the probability of the coincidental detections will be reduced by a large factor, as it would now be required that a set number of photons arrive in one phase bin. This would reduce the chances of a giant pulse like signal occurring by a factor of 64 from the probability for the 4 phase bin block. However, the expected number of coincidences would only decrease by a factor of 16, as there are four times as many phase bins as 4 phase bin blocks. This would not present a significant enough improvement to guarantee that giant pulses could be observed under most circumstances, although for 5@5, direct observations may then become possible. In conclusion, observations will probably not be able to determine the duration of gamma-ray giant pulses directly.

The giant pulse only emission mode, however, shows significant differences. The pulse profiles can be built faster than with the standard emission mode. The boosted magnitudes of the giant pulses, combined with the higher rate of occurrence outweigh the loss of the pulsed photons. This allows us to define an observational signature for this emission mode, namely a significant increase in the count of photons detected over what would be expected, and hence an increase in detection rate. Unfortunately, this could also be caused by different spectra, so remains an unclear signature.

A more definitive signature could be found in the results of SIA on the emission mode results. With the loss of the pulsed photons, the interval distribution background becomes less significant, and falls off at a slower rate. With both the increase in the number of giant pulses and the average number of photons per giant pulses, the signature peak associated with giant pulses also becomes far more pronounced. This indicates that with this emission mode, almost all photons would arrive in clusters, rather than individually.

For this emission mode, it is also probable that direct observations of giant pulses would be possible. Due to the massive pulse intensities that are required to reproduce the current data, the number of photons produced by giant pulses is very high, allowing for a high count in a four phase bin block to be set as the border required to count as a giant pulse. Additionally, the background is reduced, as pulsed photons can no longer contribute. With the high required count, and the reduced coincidence rate and a higher rate of giant pulse occurrences, the possibility of direct observation is drastically improved, which could render SIA irrelevant. The observation of a high photon count in a four phase bin block (the exact value required to count as high would have to be determined) could be used as a further signature of this emission mode.

6.0 Conclusions

6.1 General Observations

The simulated light curves shown in Section 4.1 show clearly the massive improvements that can be expected from the CTA and the possibilities offered by 5@5. The rate of data collection is massively better than the current instruments offer, and the energy range covered will allow important spectral details like the cut-off energies to be finely determined. This will allow a much more detailed view of the spectrum, allowing for the elimination or refinement of emission models. Additionally, the increased rate at which the pulse profile can be constructed will also allow for the study of the evolution of the timing of the pulsar in the gamma range, again providing more details for the development of emission models.

From the work presented here it is clear that direct imaging of giant bursts with the instruments as they stand will be achievable, but that the background will be too significant to allow for their detection in a blind search. It may be possible to investigate whether giant pulse like signals are coincidental with radio giant pulses, using the far more clearly identifiable radio giant pulses to give target times to search for gamma giant pulses, quite effectively, if a low enough count of photons is required to qualify as a giant pulse, or if only large radio giant pulses are examined. This will only provide circumstantial evidence for gamma-ray giant pulses, and will not give any data on gamma only giant pulses. This also rests on the assumption that radio and gamma giant pulses are coincidental, which is not guaranteed, as giant pulses are not necessarily visible across all frequencies.

When looking at the SIA results, one point that has to be considered is that the dead time of the arrays may prove to be longer than some of the interval bins shown here. This would mean that photons arriving within the dead time would not be seen, resulting in a decrease in the usefulness of

the SIA as a detection technique. To get round this problem, the telescopes would have to use low dead time, or even dead time free cameras. In the case of a 5@5 type array, this may be especially important to prevent loss of data from bright phenomena, as the detection rate may become too high, resulting in a significant loss of data to the dead time. The possibility of using dead time free cameras for the CTA was discussed at the CTA Collaboration meeting for the Physics Work Package in May 2010 at Zeuthen when this work was presented.

If the dead-time issue can be overcome, however, SIA is clearly a very powerful tool. It can clearly identify the presence of giant pulses when the detection rate is of the order of 0.1 Hz or greater. For 5@5 and CTA Raue and Abramowski, this level is easily achievable in the case of the Crab, even with the Fermi spectrum. 5@5 with its high effective area at low energies could presumably detect evidence of giant pulses in other more distant pulsars. The simulated results will probably not exactly correspond to an actual analysis of real data, but they provide a strong proof of concept. The flaws identified in Section 5.3 would affect the form of the signal, and would probably boost the signal, rather than compromise the method itself.

Using SIA it should be possible to determine the presence of giant pulses, and with proper study and simulations, details of their duration, frequency, magnitudes and other properties could be determined from the SIA data. Again, the limitation on the ability to pin down these properties is most likely going to be the detection rates, as this not only limits the range of magnitudes that can be detected, but determines the number of photons that will be detected per giant pulse. With a higher count of photons per giant pulse, analysis will be far more effective.

The results presented here also show that the pulse profile observational data should be able to distinguish between the two different emission modes examined, assuming the spectra of the pulsar can be firmly pinned down. Without this information, however, the signature could be obscured, as the behaviour is strongly dependant on the detection rate of the array. A clearer signal should be detectable from SIA. The increase in the strength of the SIA peak, and the decrease in the background counts should be easily detectable. The advantage of examining the SIA results for the signature, is that the signature takes the same form independent of the detection rate. Although time constraints prevented the examination of this point, direct observations of giant pulses would be another potential signature of this emission mode. With the increase in count per giant pulses, and the weakening of the background, the giant pulses should be far easier to detect.

6.2 Comparison of the Arrays

Direct comparison of the two arrays is complicated by two facts, firstly the fact that the design and performance of the CTA has not been finalised. This means we must examine best and worst case scenarios, and recognise that the actual results could be between our estimates. For the purposes of these conclusions, we will assume that the CTA built will be of the Low Energy Threshold variety, as the High Energy Threshold variant will not be able to see pulsars. Secondly, the development of the 5@5 simulations is significantly less than that of the CTA simulations, which could mean that the performance is overly optimistic. Thus, the conclusions reached in this section must be taken with a degree of caution.

The first conclusion that can be reached, is that a 5@5 type array is far better suited to observations in the GeV range than the CTA, particularly with the selection cuts currently being used in the simulations. Even the best pre-cut estimate we have, the CTA Raue estimate, the CTA cannot match the performance of the 5@5. All the analyses performed in this report for the standard emission mode show that the higher the detection rate of an array, the more effective and more rapidly the analyses can be performed. With the giant pulse only emission mode, this trend alters. For building pulse profiles, the CTA is more effective under this model, and 5@5 loses some of its resolution abilities.

It must be emphasised that the CTA array will still represent a massive improvement for pulsar observations over the current technologies, despite being optimised for observations in different energy ranges. The CTA's performance is far better than 5@5's at higher energies, which will give the CTA massive potential for observing of other phenomena in addition to pulsars. The most important recommendation for the design of the CTA with regards to pulsar observation is that the selection cuts currently used in the simulations are extremely detrimental to observations in the GeV range. An improvement in the cuts will be essential to allow the array to reach its full potential as a GeV observatory.

7.0 Extensions and Refinements

It is clear that there are several ways to take this work further. Most obviously, the current methods and models could be improved by replacing the assumptions and simplifications, such as those listed in Section 3.2, with more accurate models. Also, particularly in the case of the CTA, as the models of the arrays' performances are improved, these improvements can be used to refine the results of the simulations performed here. When a final version of the CTA is decided, for example, and its effective area simulated, this analysis could provide some interesting insights into its prospects. Details of some of these potential improvements, and of extensions beyond the current problem are given below.

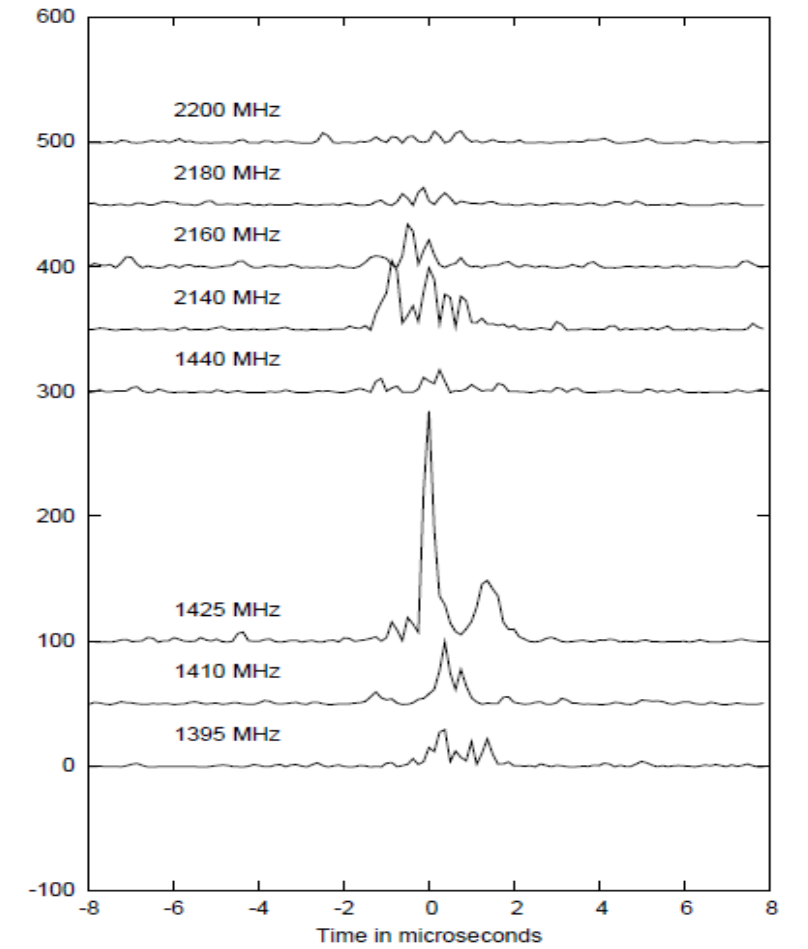
7.1 Refinements to the Current Model

As stated, the current model uses some fairly crude simplifications at points. Perhaps the most critical for the problem investigated here is the use of a rectilinear form for the giant pulses. The data available from the radio range shows us that giant pulses can have their own internal structure, as shown in Figure 24. Using the radio data available, and compensating for the broadening from the radio to gamma bands, a model could be written that produces giant pulses of a suitable form, derived from looking at the recorded radio giant pulses, and then the times of arrival of the individual photons detected during a giant pulse could be more realistically modelled. This will probably affect the Statistical Interval Analysis more heavily than any other section of the project, as this will alter the distribution of the arrival times of photons detected in giant pulses. It could potentially improve the signal of these events, as any peaks would cause photons to arrive in tighter

bunches than the assumed rectilinear form, which would improve the strength of the SIA signal, assuming the dead time issue could be overcome.

Figure 24: A giant pulse of the Crab recorded at multiple frequencies

This image shows a giant pulse that was recorded at several different radio frequencies, clearly showing an internal substructure. The different wavelengths have been shifted to allow them to be more easily seen. It can also be seen that at some frequencies, the visibility of the giant pulse is massively reduced. Image from Multifrequency Study of Giant Radio Pulses from the Crab Pulsar with the K5 VLBI Recording Terminal M. Popov et al Publications of the Astronomical Society of Japan 61, 1197-1209, 2009



To further improve the giant pulse model, a new system could be implemented for determining the duration of the giant pulses. Currently they are assigned a random time length within specified limits, with an even probability distribution, whereas the radio data suggests that the more intense pulses have a shorter duration. If a study of the relation between intensity and duration could be found or performed, the model could be adapted to produce either a randomly distributed duration or magnitude (with a suitable distribution), and a related intensity of distribution from the random value.

A study of the phases at which giant pulses occur would further refine the model. In a manner analogous to the assignment of phases for the standard photons following the Fermi light curve, the

giant pulses could then be assigned a phase based on the giant pulse distribution, rather than the total photon distribution.

One further major improvement to the simulation as a whole would be to include the changing morphology of the light curve with increasing energy. This would require a two stage improvement. Firstly a method of generating a suitable energy for each photon, with an appropriate distribution, presumably based on the pulsar's spectrum, and secondly a series of light curves for different energy bands. The exact number of bands chosen, and the relative accuracy of each, would have to be chosen dependant on the required or desired accuracy, and the available computing power required. The model would probably require wider energy ranges at higher energies, to allow the same statistical reliability of the light curves.

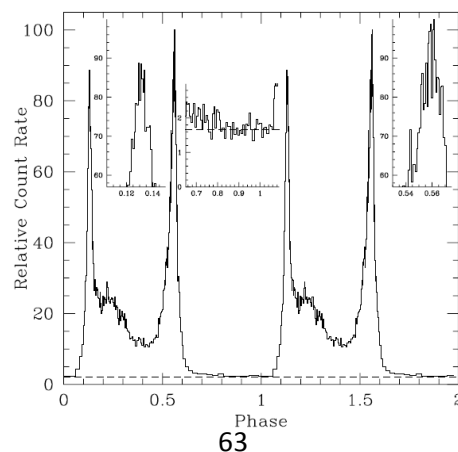
Additional work could also be done on the emission model with gamma photons only being produced during giant pulses. The model could be altered to allow different frequencies to be applied to different phase bands, which could allow the data from R. Karuppusamy, B.W. Stappers and W. van Straten (25) to be entered more accurately. The parameters that the giant pulses would have to conform to could then be determined more reliably, giving a better understanding of the signatures of this emission mode in comparison to the standard model.

7.2 Model of the Vela Pulsar

A model of the Vela pulsar could also be developed, in a very similar manner to that of the Crab model described here. Using the Fermi light curve, shown below in Figure 25, a distribution function for the phases could be developed, and swapped into the model in place of the current Crab distribution. As the Vela does not exhibit giant pulses, these would have to be omitted, by setting the frequency to zero or by removing the code entirely, and then a model of giant micro-pulses could be added to the code, using any available data on the frequency and behaviour of these phenomena.

Figure 25: Fermi pulse profile for the Vela pulsar

This pulse profile shows the results of observations in the first 8 months of the operation of the Fermi space telescope. The structure of the pulse is clear. This profile could be used to develop a model of the Vela in a similar to the manner used in the report to develop the Crab model. Image from Fermi LAT Observations of the Vela Pulsar, A. Abdo et al, 2009 The Astrophysical Journal 696 1084-1093



If the giant pulse simulator was left in the code, and the giant micro-pulse model was added, along with any other phenomena exhibited by gamma pulsars, the model could be developed as a generic gamma-ray pulsar model. As long as a distribution function could be developed for a pulsar's light curve, it could be simulated through the model, altering the frequencies and magnitudes of the phenomena exhibited, either to simulate observational possibilities, or to tie down what phenomena could be causing observed features.

7.3 Application to other Phenomena

Several other interesting phenomena, such Active Galactic Nuclei, emit in the gamma range, and these phenomena will also be visible to CTA and 5@5. The effective area curves used here could very easily be used to give estimated rates of detection for these phenomena. In addition, a model based on the Crab model used here could be developed to investigate at what level transient phenomena could be observed, as a function of duration and magnitude. In addition, any short term bright phenomena could be detected by applying SIA to the observational data from these phenomena.

The Statistical Interval Analysis could prove useful in observations of any phenomena which exhibit behaviours of a short term nature which increase the intensity of the object where the detection rate is too low to allow the direct observation of these events. Obvious applications are high energy astrophysical observations, where the rate of detection is limited by the rarity of the high energy photons, or satellite experiments where the count rate is limited by the small effective areas of the telescopes. For SIA to function, the only requirement is that the events cause a sufficient increase in intensity to allow for the detection of two or more photons from one event. The greater the rate at which the events occur, and the greater the average number of photons detected per event, the clearer an SIA signal will become.

Another interesting application could be the search for dark matter, and dark matter clumps and other structures. The popular dark matter models predict that dark matter should produce gamma rays, with the energy of these gamma-rays being dependant on the mass of the dark matter particles. The current energy range of possible masses is broad, between 100 GeV and 10 TeV. The mass is roughly the maximum gamma-ray energy that could be produced, so using either the CTA or 5@5 to observe dark matter candidate objects could give evidence for the mass of dark matter particles, allowing the refinement of our models. With the increased effective area and sensitivity in comparison to current technologies, the arrays would also allow more detailed examination for structures and sources, allowing a better understanding of the distribution of dark matter in the galaxy.

Acknowledgments

I would like to thank the members of the University of Hamburg Astroparticle Physics group, in particular my fellow inhabitants of room 14, for their help, guidance and support during this work, especially their toleration of my endless questions and horrific German. I would also like to thank Professor D. Horns, for his input and suggestions, as well as for giving me the opportunity to both work in his group on this topic, and to present this work at a conference. Finally, I would like to thank my fellow Erasmus students, who have proof read this work, and who have provided encouragement, motivation and healthy competition during the year. I would also like to thank Professor Loparco of the Fermi LAT Collaboration, for his assistance and suggestions with regards to reconstructing the Fermi pulse profile data. This work made extensive use of the arXiv and NASA ADS systems.

Bibliography

1. Fred Lawrence Whipple Observatory. *Wikipedia*. [Online] [Cited: 10 April 2010.] http://en.wikipedia.org/wiki/Fred_Lawrence_Whipple_Observatory.
2. IACT. *Wikipedia*. [Online] [Cited: 10 April 2010.] <http://en.wikipedia.org/wiki/IACT>.
3. **Hewish, A et al.** Observation of a Rapidly Pulsating Radio Source. *Nature*. 1968, Vols. 217 pp 709-713.
4. **Fermi LAT collaboration.** The First Fermi Large Area Telescope Catalog of Gamma-ray Pulsars. *Astrophysical Journal Supplement*. 187, 2010, pp.
5. **Aliu, E et al.** Observation of Pulsed Gamma-Rays Above 25 GeV from the Crab Pulsar with MAGIC. *Science*. 2008, Vol. 322, pp 1221-1224.
6. **Guillemot, L. on behalf of the Fermi LAT Collaboration.** Pulsar Observations with the Fermi LAT: what we have seen. *2009 Fermi Symposium*. Washington D.C. : s.n., 2009 November 2-5.
7. **Abdo, et al.** The Large Area Telescope on the Fermi Gamma Ray Space Telescope Mission. *The Astrophysical Journal*. 2009, Vol. 697, Issue 2, pp. 1071-1102.
8. **Schoenfelder, Volker and (Ed).** *The Universe in Gamma Rays*. Berlin Heidelberg : Springer, 2001.
9. The HEGRA Atmospheric Cherenkov Telescope System. *Max-Planck-Institut für Kernphysik*. [Online] Max-Planck-Institut für Kernphysik. [Cited: 2 May 2010.] <http://www.mpi-hd.mpg.de/hfm/CT/CT.html>.
10. **W. Hofmann, et al.** Comparison of techniques to reconstruct VHE gamma-ray showers from multiple stereoscopic Cherenkov images. *Physics*. 1999, Vol. 12, 3 pp 135-143.
11. **Lyne, Andrew G and Graham-Smith, Francis.** *Pulsar Astronomy (Second Edition)*. s.l. : Cambridge Astrophysics Series .
12. **A. Abdo, et al.** The Vela Pulsar: Results from the First Year of FERMI LAT Observations. *The Astrophysical Journal*. 2010, Vol. 713, pp 154-165.
13. Cherenkov Telescope Array. *Cherenkov Telescope Array Home*. [Online] CTA Collaboration. [Cited: 2 May 2010.] http://www.cta-observatory.org/CTA_home.html.
14. **Aharoniana, F.A.** 5@5 – a 5 GeV energy threshold array of imaging atmospheric Cherenkov telescopes at 5 km altitude . *Astroparticle Physics*. 2001, Vol. 15, 4 pp 335-356.
15. **Lyne, A.G., Pritchard, R.S. and Smith, F.G.** 23 years of Crab Pulsar rotational history. *Monthly News of the Royal Astronomical Society*. 1993, Vol. 265, pp 1003-1012.
16. **Abdo, A et al.** Fermi Large Area Telescope Observations of the Crab Pulsar And Nebula. *The Astrophysical Journal*. 2010, Vol. 708, 2 pp. 1254-1267.
17. **Stappers, M.V. Popov and B.** Statistical properties of giant pulses from the Crab pulsar. *Astronomy & Astrophysics*. 2007, Vol. 470, pp 1003-1007.

18. **Manchester, R. N., Hobbs, G. B., Teoh, A. Hobbs, M.** The Australia Telescope National Facility Pulsar Catalogue. *Astrophysical Journal*. 1993-2006 (2005), Vol. 129, <http://www.atnf.csiro.au/research/pulsar/psrcat/>.
19. **Simon Johnston, Willem van Straten, Michael Kramer, Matthew Bailes.** High Time Resolution Observations of the Vela Pulsar. *The Astrophysical Journal*. 549, 2001, pp 101-104.
20. **Bilous A. V., Kondratiev V.I., Popov M.V., and Soglasnov V.A.** Review of overall parameters of giant radio pulses from the Crab pulsar and B1937+21. *AIP Conference Proceedings*. 2008, Vol. 983, 1.
21. **Logvinenko, T.V. Smirnova and S.V.** Giant Pulses of PSR B0531+21 at 112 MHz. *Astronomy Reports*. 2009, Vol. 53, No. 4 pp 334-342.
22. **Collaboration, The CTA.** Wp mc production config. *CTA Wikipages*. [Online] [Cited: 12 November 2009.] http://www.cta-observatory.org/ctawpcwiki/index.php/Wp_mc_production_config.
23. **Abramowski, A et al.** Locating the VHE source in the Galactic Centre with milli-arcsecond accuracy. *Monthly News of the Royal Astronomical Society*. 2010, Vol. 402, 2 pp 1342-1348.
24. **Raue, M and Mazin, D.** *Astroparticle Physics*. Submitted, 2010.
25. **R. Karuppusamy, B.W. Stappers and W. van Straten.** Giant pulses from the Crab pulsar- A wide band study. *Astronomy & Astrophysics*. Submitted April 2010.

Appendix I: Simulated Light Curves

Figure 1: Simulated light curve of 50 hours of observation with CTA LET

As can be seen, even after 50 hours of observations, the signal from the pulsar is completely obscured in the noise in the system. Given the low duty cycle of Cherenkov telescopes, this represents a significant period of observation. This makes the CTA LET impractical for pulsar observations.

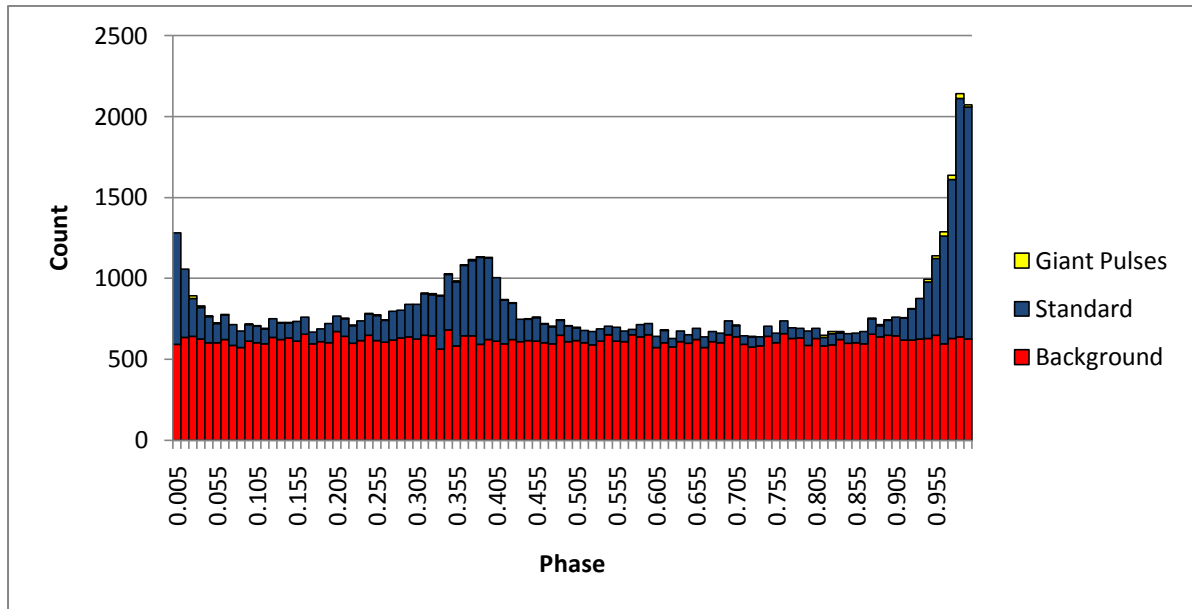


Figure 2: Simulated light curve for 0.5 hours of observation of the Fermi normalised MAGIC decay with CTA LET

The increased detection rate has a significant impact on the clarity of the results. Here both the P1 and P2 peaks are very clear. It should be noted that this spectrum is the most optimistic of the cases, and should therefore be regarded as a limiting case.

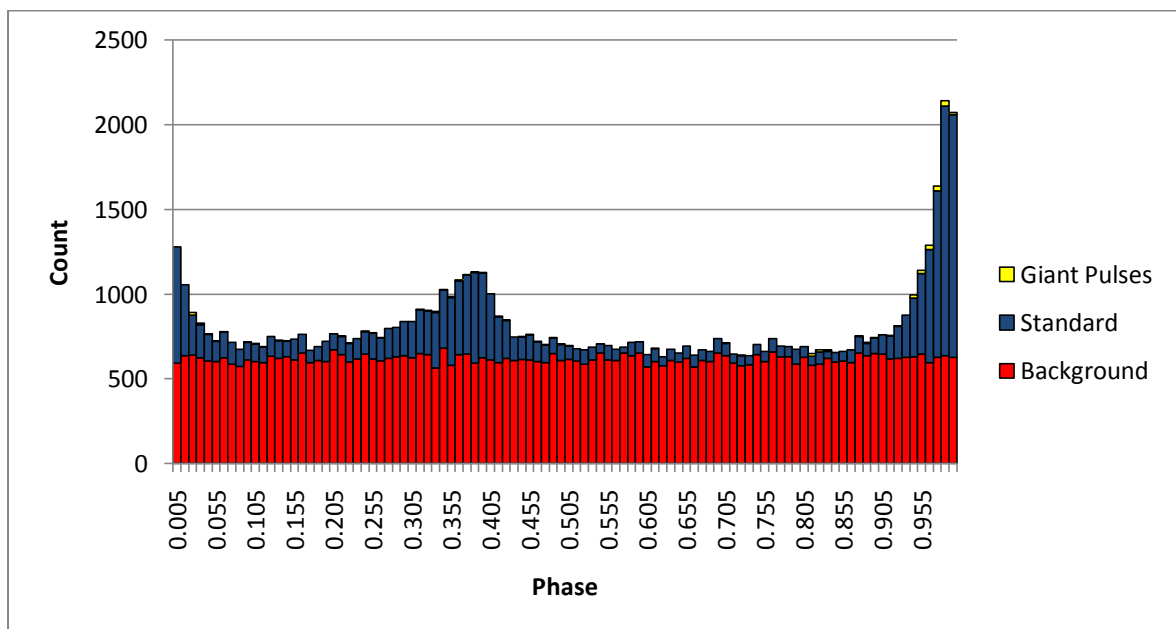
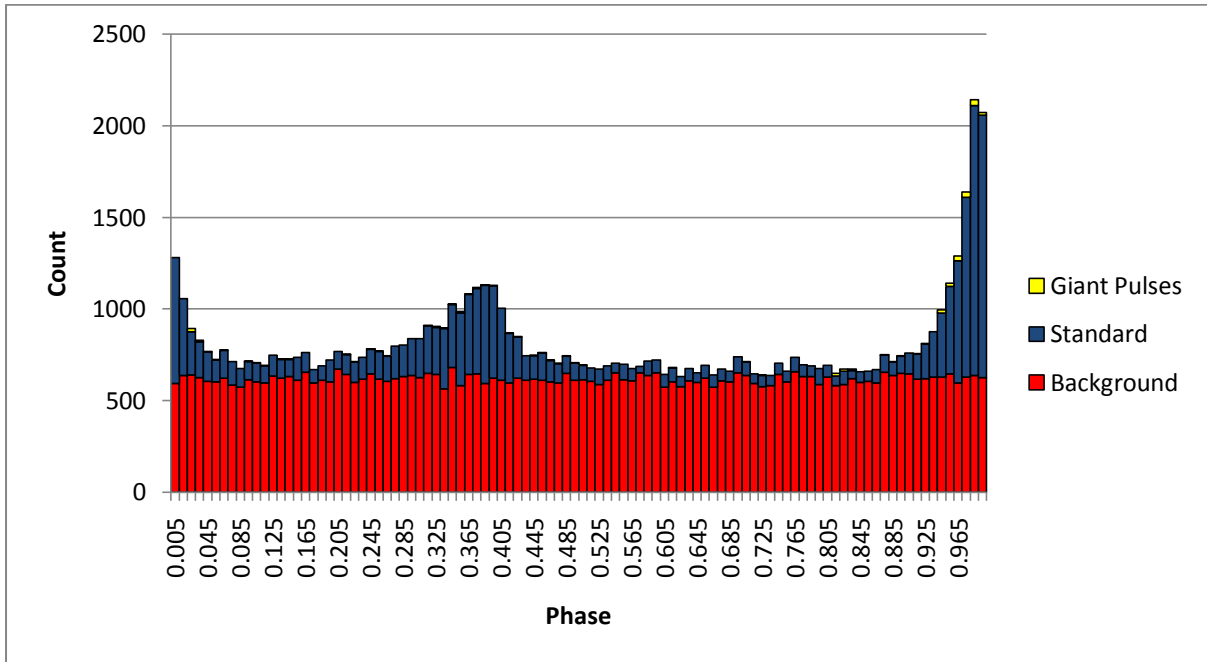


Figure 3: Simulated light curve for 5 hours of observations of the MAGIC spectrum with CTA Abramowski

This curve clearly shows that after 5 hours, the details of the pulse are very well defined. This plot also shows well the clustering of the giant pulses in the P1 and P2 peaks. This pulse profile could conceivably be achieved in a night or two's worth of observations.



Appendix II: Statistical Interval Analysis

Figure 1: Results of SIA on 25 hours of observations of the Fermi spectrum with CTA LET

The data here clearly shows no useful information. The giant pulses have not produced more than one photon each, which means that there is no signal for the SIA to detect.

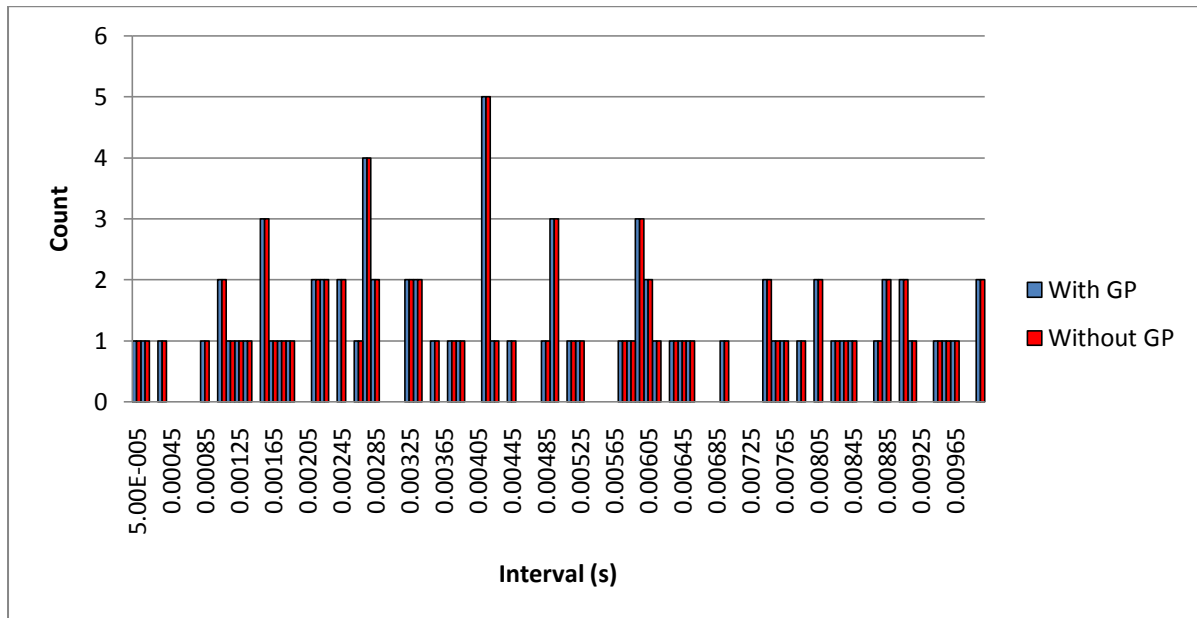


Figure 2: Results of SIA on 10 hours of observations of the Fermi normalised MAGIC decay with CTA LET

The spike associated with the giant pulses here is very clearly visible. As the background rates are low, the detections have a much greater significance in comparison. As the spectrum used here is the most optimistic case, this represents the best possible results that could be expected from the CTA LET.

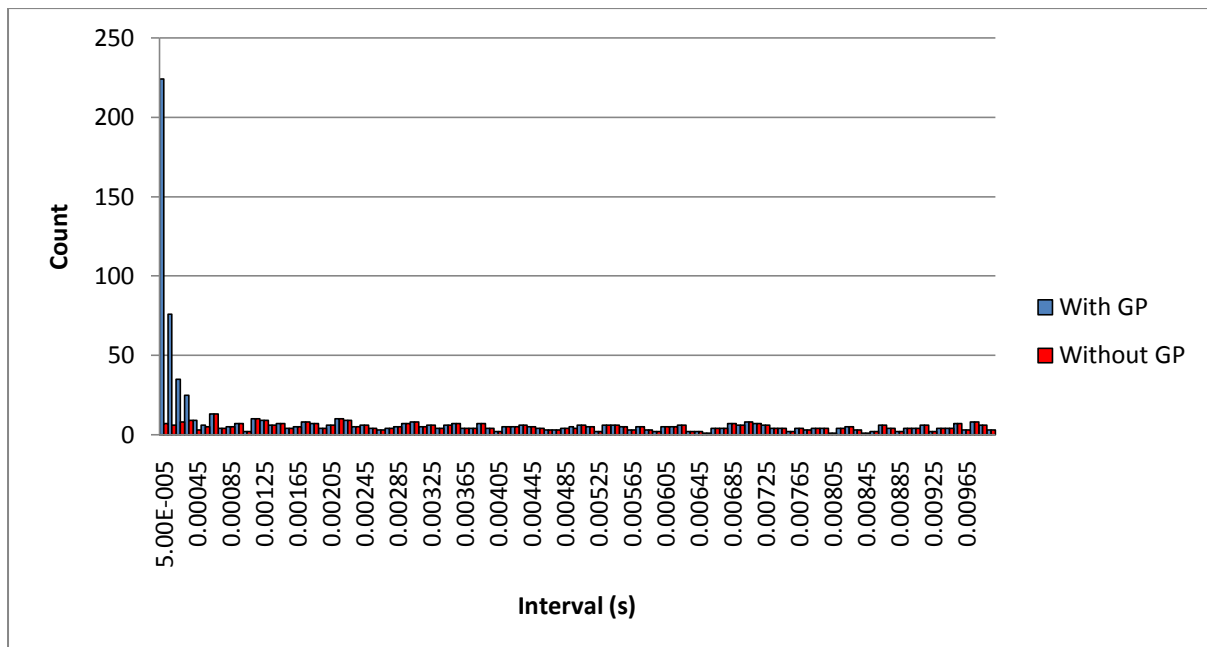


Figure 3: Results of SIA on 10 hours of observation of the MAGIC spectrum with CTA Abramowski

The signal expected from giant pulses is clearly visible here. With an excess of about 130 counts, or around 10 times the variation in the system, this signal would be very easily picked out, allowing for an easy detection after only a few nights observations.

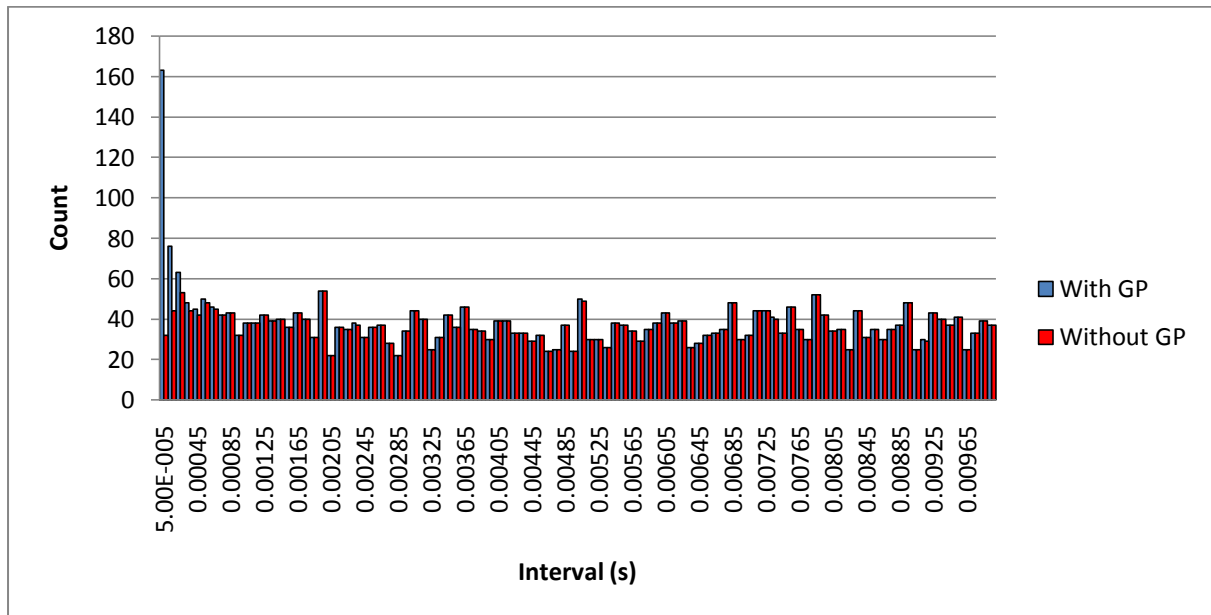


Figure 4: Results of SIA on 0.5 hours of observations of the Fermi normalised MAGIC decay with CTA Abramowski

The enhancement of the signal due to the higher detection rate is demonstrated in the comparison to Figure 3. Here the excess at about 4000 results is hundreds of times larger than the variation, which is barely visible on this graph. What can also be seen clearly is the decaying distribution of the intervals that are not due to the giant pulses.

